Review

Fully printed organic solar cells – a review of techniques, challenges and their solutions

S. Ganesan [a,b,c,1], S. Mehta [a,1], D. Gupta [a,*,1]

[a] Department of Metallurgical Engineering and Materials Science, IIT Bombay, Mumbai, 400076, India
[b] Department of chemical engineering, Monash University, Australia
[c] IITB-Monash research academy, Mumbai, 400076, India

ABSTRACT

The emergence of solar cells on flexible and bendable substrates has made the printing process a ubiquitous tool for the fabrication of these devices. The various printing techniques available now such as inkjet, screen and flexography offer cost-effectiveness, user-friendliness and suitability for mass production. While downscaling the fill factor and efficiency of organic solar cells. A multilayered structure, the combination of different printing techniques avails the variety of thickness and resolution required for each layer in the production of an organic solar cell. In this review article, we discuss the suitability of the inkjet and screen printing processes to produce organic solar cells. We also discuss various challenges involved in the fabrication of organic solar cells using these two techniques and the possible solutions for the same. We also provide an analogy that both processes share. Further, we consider future possibilities of combining these printing technologies to produce organic solar cells to improve device performance.

© 2019 Association of Polish Electrical Engineers (SEP). Published by Elsevier B.V. All rights reserved.

Contents

---

* Corresponding author.
  E-mail address: diptig@iitb.ac.in (D. Gupta).
[1] These authors contributed equally to this work.

1. Introduction

The conventional electronics with its elements such as resistors, capacitors and inductors fitted in a box with a plug is fading away. A new revolution of printed electronics is emerging where scientists produce functional devices on flexible polymer substrates such as PET, paper and textiles. Thus, presenting a new era of flexible and bendable smart devices. Besides printing paints or different colours, there have been significant advancements in the printing of various functional materials (metal inks, dielectric materials and semiconductors), as well as biological molecules (proteins, extracellular matrix) or cells (human cells or microbial cells) [1,2]. These materials thus printed can be employed for several applications such as organic solar cell (OSC), sensors, transistors, batteries, light-emitting diodes, sensors and in tissue engineering [3]. The demand for mass fabrication and a wide range of materials (inks and substrates) gave a new paradigm to the solar cell market, presented a way towards printed organic solar cells (pOSC). The further challenge is to get the characteristics comparable to the ones fabricated from conventional techniques. The traditional methods used for fabrication of solar cells, such as thermal evaporation and spin coating, are not compatible with the mass production of these devices and are also responsible for up raising the cost of organic solar cell production [4]. pOSCs are fabricated in two geometries: normal and inverted geometry, as shown in Fig. 1. The photoactive layer in pOSC is a blend which consists of a donor with high ionization energy and an acceptor material high electron affinity. The donor of the active layer blend generates the electron-hole pair called excitons when light falls on it. These excitons migrate to the donor-acceptor interface by diffusion, where they get separated into electrons and holes and finally transfer to the respective electrodes. The intermediate hole and electron transport layers between the photoactive layer and the electrodes help in enhancing the mobility of these charge carriers (electrons and holes) [5].

2. Different printing techniques

We can classify printing techniques into two categories: conventional printing such as letterpress, screen, flexography, offset and gravure, and digital printing techniques such as inkjet and laser printing. In the area of printed electronics, technologies such as screen printing, inkjet printing, flexography and gravure printing are among the widely used ones. Also, according to the IDTechEx

[6], towards commercialization, 98% of the printed electronics job is carried out by screen printing and the remaining 2% is by other methods such as coating, inkjet, flexo and gravure printing and these are limited to research and development purposes only [6]. Table 1 provides a brief comparison of these techniques.

The objective of this review article is to provide a brief general introduction of inkjet and screen-printing techniques to the readers and how we utilize these techniques in the production of OSCs. There are already available many review articles illustrating the fabrication techniques for organic solar cells and their performances. Here, we describe explicitly the different kind of substrate used for these devices, inks for various layers and various printing parameters used for the fabrication of each layer to understand the current state of the art in the area of pOSC.

2.1. Inkjet printing

Inkjet printing is an emerging technology for the manufacturing of microscale components, where we print minute droplets of ink over the substrate in the lateral direction [7]. The direct patterning and conservation of materials make this technique fascinating for the fabrication of OSCs. The essential ink requirements for the ink to be used for inkjet printing involves the optimization of several physical parameters such as density, viscosity and surface tension of the ink. Fromm developed the dimensionless number Z, which is the inverse of Ohnesorge number, to investigate the stable drop formation [8]. The Z number which is the ratio between Reynold's number and the square root of the Weber number is given by:

$$Z = \frac{\sqrt{\rho \gamma L}}{\eta}. \tag{1}$$

Where, γ is the surface tension in mN/m, η is the viscosity in mPa S, ρ is the density in kg/m^3 and L is the diameter of the tube in μm.

The modeling of the drop formation in inkjet printing estimated that Z value should lie between 1 and 10 for a printable fluid [9]. Below the lower limit, there is no drop formation due to the pressure pulse dissipation of the viscous forces, and above the upper limit, satellite drop formation arises.

The uniformity of the printed pattern depends upon the distance between the substrate and the nozzle termed as Mean standoff distance (MSD). A satellite drop accompanies the main drop for smaller MSD, where larger MSD result into an unstable and inaccurate deposition. [10] The diameter and volume of the ejecting droplets
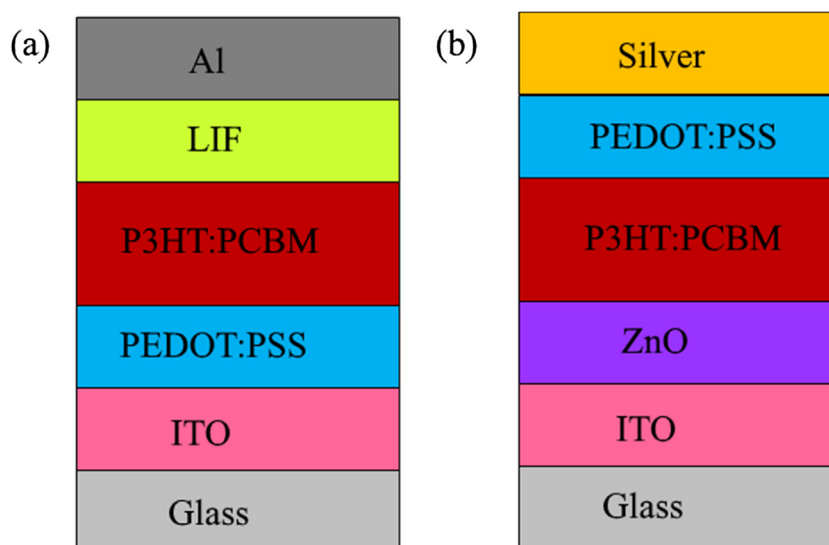

Fig. 1. Geometry of (a) normal and (b) inverted printed organic solar cell.

Table 1
Comparison of different printing processes [7].

S.No	Printing process	Viscosity Pa S	The thickness of printed line μm	The width of printed line μm	Resolution μm
1.	Offset	1 to 10	0.5 -1.5	10	80
2.	Screen	0.5 to 5	Upto 12 μm	30-50	100
3.	Flexography	0.05-0.2	0.8 to 1	45 to 100	50
4.	Gravure	0.05 to 0.2	0.8 to 0.5	10 to 50	30
5.	Inkjet	0.005 to 0.02	<0.5	30-50	20

with the same nozzle diameter can be controlled by applying a sequence of positive and negative pressure pulses and by modulating the input voltage waveform. In addition to that, drop spacing also plays a significant role in defining the thickness and quality (edge sharpness) of the printed pattern [11]. Thus, efficient inkjet printing involves the ink preparation and optimization of printing parameters. Even after achieving these, there are challenges involved in this process described in the next section.

2.1.1. Challenges in inkjet printing

In inkjet printing, the printed droplets merge to form a uniform continuous film and annealing of this film is carried out at the next step. The capillary flow and contact line pinning associated with the droplet evaporation leads to the coffee ring effect. We can visualize it as a build-up of the solute at the periphery of the drop driven by the flux of fluid during evaporation [12]. This effect is considered as a significant challenge in the printed devices and hence affect their performances. To nullify this effect, researchers use hydro soluble polymer additives, dual solvents, or manipulate the substrate temperature with a single solvent. Employing the use of Marangoni flow [13], the ellipsoid particles [14], decreasing the substrate temperature [15] addition of high boiling point solvent [16] and helps in minimizing the coffee ring effect.

Another challenge in inkjet printing is uniformity of inkjet-printed line, which forms as a result of merging of drops ejected from the nozzle with the applied voltage waveforms [17]. The diameter and centre to centre spacing (drop spacing) determine this uniformity of the ejecting drops. Drop spacing smaller than the drop diameter results into the bulging of lines, whereas a larger drop spacing leads to the non-uniform printed lines. The spreading of the ejecting ink drop depends on the surface tension of the ink and the surface energy of the substrate [18].

The other challenges in inkjet printing involve viscosity limitations, as the manipulation of the functional inks for meeting up with the viscosity requirements of inkjet printer affects their desirable properties. Another most significant challenge involved is nozzle clogging, where the size and non-homogeneous distribution of solute particles in the ink results into the nozzle clogging of the print head of inkjet printer [19].

2.2. Screen printing

This printing technique builds upon a screen, which is a woven mesh (either cloth or steel). A non-permeable material covers the unwanted areas in the mesh and ink is pushed through the remaining regions onto the substrate with a squeeze [20]. Screen printing is the best method for large area printing with significant speed on a variety of substrates, especially when the final printed thickness required is substantial.

The viscosity of screen printing must be high ($\sim$1 Pa S). Moreover, it should exhibit shear-thinning behaviour to allow the smooth flow of ink through the mesh during printing. Further, it should regain its viscosity values after hitting the substrate, to prevent the lateral spreading of the ink. Mesh count, squeeze angle, squeeze pressure and squeeze speed can determine the volume of the ink deposited. Further, the distance set between the substrate

and the mesh, known as snap-off distance, also decides the fidelity of the printed pattern [21].

Hence, like inkjet printing, successful screen printing also depends on the ink preparation and optimization of printing parameters. Again, this process also involves several challenges mentioned in the next section.

2.2.1. Challenges in screen printing

The main problem with screen printing technique is the mesh markings observed in the printed films. The possible reasons for such mesh markings are ink rheology, thread diameter in the mesh and screen tension. A meniscus, which is the source of extra ink forms underneath the mesh during printing. Reducing the meniscus formation by using a mesh with smaller thread diameter, allowing the leveling of the ink as fast as possible (by decreasing the viscosity and increasing the surface tension of the ink) or increasing the screen tension helps in minimizing the mesh markings. Further, the tension experienced by the mesh stretched over a frame- also termed as screen tension can also be the possible reason for mesh markings [22]. The higher tension gives less chance for the mesh to hang around in ink and hence less mesh marking in print. Another challenge in screen printing is wastage of an enormous amount of ink as only 70% of the ink is deposited on the substrate and rest 30% get wasted in the mesh itself. Also, the thickness of the screen-printed film is usually in the range of 500 nm–1000 nm. Therefore, it is generally required to play with the printing parameters to get printed thickness adequate for solar cell applications [23].

2.3. Analogy of both the techniques - inkjet and screen printing

Performing the analogy of screen printing with inkjet printing, the mesh in screen printing plays the role same as the nozzle in inkjet printing. The mesh count in screen printing and nozzle diameter in inkjet is also taken into consideration while defining ink composition (mainly particle size) and these parameters also determine the ink volume. Further, as elements associated with piezoelectric (jetting voltage, frequency, pressure and waveform) helps in controlling the ejected drop volume in inkjet. The squeeze parameters such as angle, speed, pressure and material allow controlling the screen-printed ink volume. The inkjet and screen-printing processes are carried out by specifying a well-defined distance between the substrate and source for ink dispensing (nozzle in case of inkjet and mesh in case of screen printing). Fig. 2 provides the complete analogy of both the processes described here.

Followed by a brief introduction of inkjet and screen-printing techniques, their challenges, as well analogy, we will discuss the use of these techniques for OSCs in the subsequent sections. These will involve the substrates for printing processes as well as printable inks for different layers of OSCs.

3. Printing of organic solar cell layers

3.1. Substrates for solar cells

In an OSC, a photoactive layer is sandwiched between two electrodes. One is the low work function opaque electrode such as
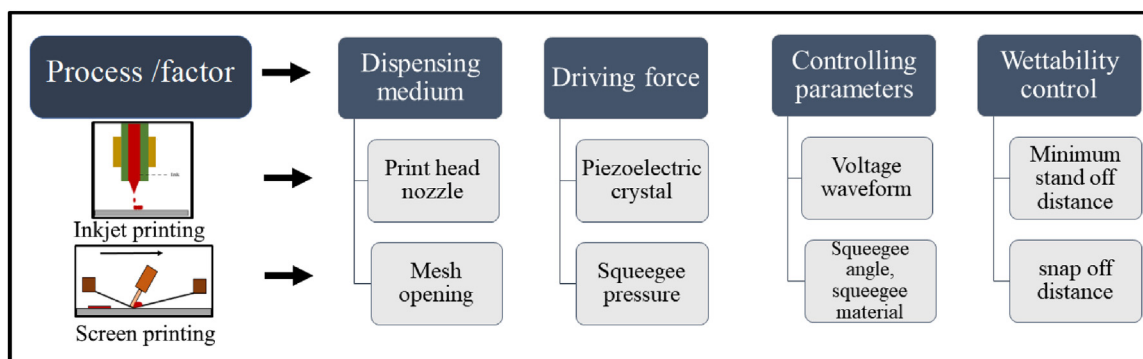
Fig. 2. Smart art showing the analogy of inkjet and screen printing.

aluminum and the other is the transparent electrodes which allows the sunlight to pass through. While selecting a substrate for pOSC, the major things need to be taken into consideration include transparency, proper adhesion to the organic conducting layer, as well as the compatibility of the substrate material with the solvents used in the processing methods of various layers.

The glass is the most commonly used substrates for pOSC [24]. But it doesn't provide the flexibility or bendability to the devices made on them and hence restricts their use in certain applications. But these substrates are suitable for pOSC involving the layers which require high processing temperatures such as solution processed ITO, IZTO [25,26]. Polymers such as PET, PEN and polycarbonate have also been used as a substrate for printed electronics [27]. These substrates are quite compatible with the processing temperatures of most of the polymers used in the pOSC. Paper is another preferred substrate for OSCs because of flexibility, low cost, eco-friendliness, recyclability and compatibility with conventional and digital printing machines. The use of lightweight, inexpensive and biodegradable paper as a substrate for pOSC can enable the low-cost and flexible polymer solar cells [28]. Besides the advantages of using paper as a substrate, there are also challenges involved with this. Some of these are high roughness, poor tensile strength, poor resistance to chemicals and the suction of liquids due to capillary action [29].

Further, the use of substrate such as steel for pOSC has the significant potential to increase the capability of OSC, since the devices, thus made can be implanted at the roof top of the houses in the rural areas, in automobiles and spaceships [30]. OSC fabricated on the steel substrate and the structure of the device are shown in Fig. 3(a) and 3(b). Moreover, for every substrate, in order to get the proper adhesion of printed layers, there is a requirement of surface treatments which can be accomplished by using plasma cleaning, UV ozone cleaning or by chemical treatments such as silanization and piranha treatment [31]. In addition to that, the substrate for solar cells should also have a low coefficient of thermal expansion so that the post-processing doesn't affect it. High tensile strength is another property required for pOSC substrate. It should also be resistant to chemicals and solvents used for different layers. Fur-

ther, in order to avoid degradation, it should be impermeable to oxygen and moisture. It should also be smooth and clean for providing uniformity and proper adhesion [32].

3.2. Printing of organic solar cell layers

Different layers of the organic solar cell and their fabrication by printing techniques, mainly inkjet and screen printing are discussed in this section. The parameters employed in the printing of these layers and their influence on the device performance are also mentioned.

3.2.1. Transparent electrode

We start with the transparent electrode, indium tin oxide, where the light enters the solar cell. Indium tin oxide (ITO), indium zinc tin oxide (IZTO) and antimony doped tin oxide(ATO) are some of the materials used as a transparent electrode in the production of OSCs [33,34]. ITO is the most preferred transparent electrode by the researchers because of high optical transmittance and low sheet resistance [34]. The main challenge in the printing of ITO is the higher sheet resistance of the printed layer, which is overcome by using a silver grid/ITO composite. Alternatively, conductive metal oxide-carbon complex, such as indium tin oxide/ graphene hybrid film is also used to reduce the sheet resistance of the ITO upto 10% [35]. Another problem with ITO is the requirement for sintering at a very high temperature which is being overcome by using alternative methods of sintering such as microwave sintering.

This is because sintering in conventional hot oven sintering, sintering temperature (above 200 °C) and time duration for sintering are high (>60 min) making it unsuitable for fast industrial production [36]. Whereas in microwave sintering, sintering can be performed at a lower temperature time in a short time duration (<5 min). Also, in microwave sintering there is selective absorption of the microwave radiation by indium tin oxide particles and it is not absorbed by the base substrate. Another advantage of microwave sintering is the volumetric heating where the entire volume of the sample is heated the same time. Fig. 4(a) and 4(b)
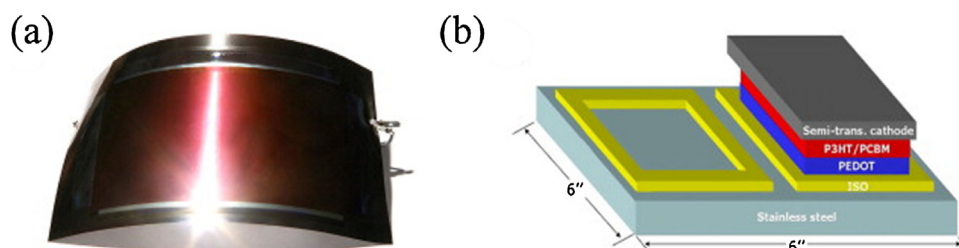

Fig. 3. (a) organic solar cells fabricated on (a) steel substrate and (b) structure of the fabricated solar cell [30].
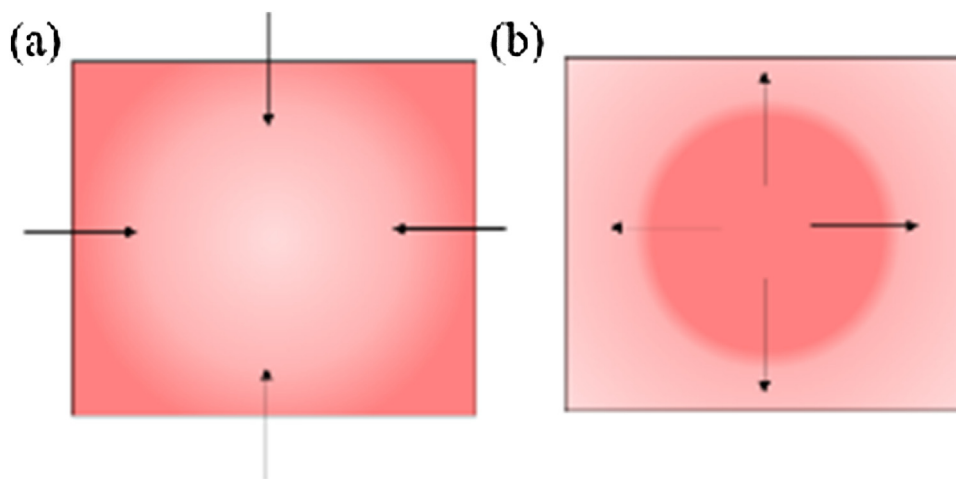
Fig. 4. (a) conduction of heat in conventional hot oven (b) conduction of heat in a microwave oven [37].

Table 2
Comparison between inkjet printing and screen printing of ITO films [34–42].

Printing process	Parameters that influence the thickness	Annealing method	Sheet resistance	Optical transmittance	Efficiency
Inkjet printing	Printing speed, drop overlap ratio [39], drop volume, multiple layers	Hot plate oven (400 °C) (or) microwave radiation (200 °C)	Without grids (200 $\Omega/\square$) with silver grids (1.5 to 3 $\Omega/\square$)	Without grids > 84%. With grids < 82 %	2.13 %
Screen printing	Squeegee pressure, the speed of the squeegee, mesh dimension, screen tension, snap off distance and paste viscosity. [41]	Hotplate (120 °C) for 5 to 10 min for drying and IR furnace (600 °C for 40 min)	5 to 10 k ohms	< 80 %	0.0013 %

shows the working principle of hot plate oven and the microwave oven. In the hot plate oven, the heat is transferred from the edge of the sample to the center by conduction and there is non-uniform heating [37]. In microwave sintering, the microwaves are absorbed by the sample and the polar molecules having positive and negative charge in opposite ends rotate according to the alternating field from the microwaves and produce thermal energy by dielectric heating [38]. The spread of the heat in a microwave oven is from the center to outside as shown in Fig. 4(b).

Inkjet printing of ITO is carried out by controlling overlap ratio and printing speed to achieve an ITO layer of thickness 750 nm. This printed ITO ink is then sintered at high temperatures (approx450 °C) in a nitrogen atmosphere. The inkjet printed zinc oxide had a sheet resistance and optical transmittance of 200 $\Omega/\square$ and 85% respectively [39]. The efficiency of the OSCs fabricated over inkjet printed ITO in normal geometry (Glass/inkjet printed Indium tin oxide / PEDOT: PSS / P3HT:PCBM / Ca/Al) was found to be 2.13%. This efficiency value was less than the devices fabricated over lithographically patterned ITO [38], as the sheet resistance of the Indium tin oxide films printed by inkjet printing was considerably higher (200 $\Omega/\square$) than the sputtered ITO (7.6 $\Omega/\square$). This can be circumvented by introducing silver grids and sandwiching these between two inkjet printed ITO thin films [39]. The optical transmittance and the sheet resistance of the transparent electrode assembly, ITO (1000 nm /silver grid (100 nm)/(ITO) 1000 nm composite electrode), was 83.72% and 1.42 ohms/square, respectively [40].

In screen printing, the parameters which influence the thickness of the deposited screen-printed ITO films are the speed of the squeegee, screen tension, snap off distance, paste viscosity and mesh dimension. The thickness of the screen-printed ITO films are in the range of 10–30 μm [41]. These films are then post processed by annealing (for a duration of 10–15 min at 120 °C) to remove solvents and enhance adhesion and further fired in an IR furnace (at

600 °C for 40 min) to provide crystallization of the films [42]. The screen-printed films are found to have a grain size of 12 nm and sheet resistance in the range of 5000–10000 ohms [42]. Comparison between the inkjet printing and the screen-printing process for printing indium tin oxide in terms of printing parameters, annealing, sheet resistance, optical transmittance and the efficiency is shown in Table 2.

3.2.2. Hole transport layer (HTL)

Hole Transport layer (HTL) is an anode buffer layer which favours the movement of holes and blocks the movement of electrons. The functions of the anode buffer layer are to provide an ohmic contact with the donor material, to transport the positive charge carriers and to block the negative charge carriers. In addition to that the buffer layer reduces the roughness of the substrate and prevent the penetration of solvents from the top electrode onto the active layer [43]. The anode buffer layer also acts as an optical spacer by improving the photon absorption. Metal oxides such as nickel oxide, molybdenum trioxide (MoO_3), tungsten trioxide (WO_3), vanadium(V)oxide(V_2O_5), ruthenium(IV) oxide (RuO_2), copper oxides(CuOx), chromium oxides(CrOx), polyethylene Diethoxy Thiophene- polystyrene Sulfonate (PEDOT: PSS), graphene oxide were some of the materials which were used as the hole transport layer [44,45].

Among the available HTLs, PEDOT:PSS is extensively used because of 1) its high optical transmittance (>80%) facilitating the movement of light in the form of photons, 2) high hole mobility (20 cm^2/V/s) to achieve immediate transfer of holes generated in the photo-activated layer to the anode through HTL preventing the charge recombination. And hence promoting the uphill movement of the holes by proper alignment of the energy levels [46]. PEDOT:PSS is a non-Newtonian liquid with high molecular weight and viscosity [47]. In order to be used for inkjet printing, it is diluted by DI water (generally in the ratio 1:3) to prevent nozzle clogging.
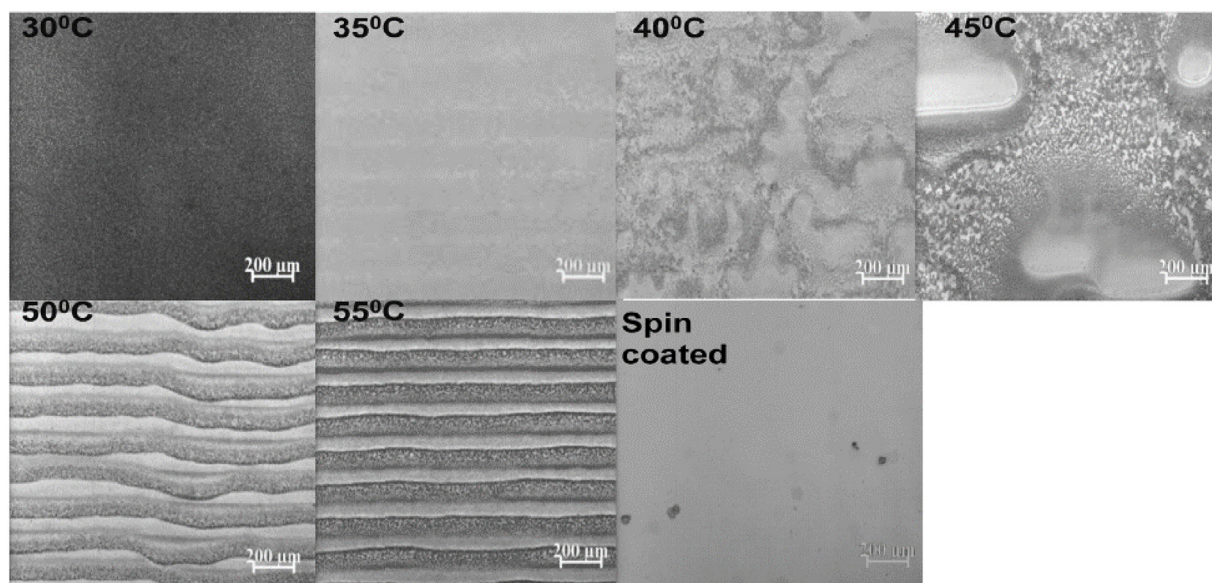
Fig. 5. Influence of different substrate temperatures from 30 °C to 55 °C at an interval of 5 °C on the inkjet printed PEDOT:PSS thin films. The last image is spin coated PEDOT:PSS film [48].

The wettability of PEDOT:PSS over the glass and other polymer substrates can be improved by using surface treatment methods such as oxygen plasma and corona treatment [48].

For inkjet printing PEDOT:PSS, drop spacing in the range of 25 μm–30 μm resulted into print film thickness in the range 5–27 nm. The uniform inkjet printed PEDOT:PSS thin film was attained at a substrate temperature range of 30–35 °C, whereas higher temperature (above 45 °C) leads to nozzle clogging and decreased drop diameter due to rapid evaporation [48]. Hence there was no uniform film formation above 30 °C as shown in Fig. 5.

Further, annealing temperature of the films is optimized in terms of surface roughness at a temperature. For PEDOT: PSS, it is estimated to be 120 °C for 20 min as the inkjet printed film surface roughness was found to be minimized (4–5 nm) at this temperature [49]. Moreover, the efficiency of the OSCs produced over inkjet printed PEDOT: PSS was in the range of 2 to 3 % [49–51]. Which is 10% less than the spin-coated devices. This is because of a low fill factor in inkjet-printed devices, which is due to variations in printed film thickness resulting in improper morphology. Improper morphology affects the mobility of the charge carriers resulting in a low fill factor. The conductivity of the PEDOT:PSS thin film is very low (∼1 S/cm). To improve the conductivity of PEDOT: PSS, solvent additives such as sorbitol, ethylene glycol, dimethyl sulfoxide, dimethyl sulfate, polyethylene glycol and Triton-X-100 (surfactant) are added [52]. The solvent additives transform the benzoid structure of PEDOT to quinoid structure and a closely packed crystalline structure is formed [53]. For example, the specific conductance of the inkjet printed PEDOT: PSS thin film was improved from

7.82×10^{-1} S/cm to 1.52×10^2 S/cm by the addition of glycerol and it is improved further by the addition of Ethylene Glycol Butyl Ether (EGBE) to 1.64×10^2 S/cm. [50] Addition of solvent additives 6% glycerol and 0.2% ethylene glycol butyl ether to PEDOT: PSS improved the efficiency of P3HT:PCBM based devices from 2.09% to 3.16%. A higher fill factor and short circuit current density were noticed after the inclusion of glycerol and ethylene glycol due to the enhancement in the surface morphology.

For screen printing PEDOT:PSS, a 165 mesh screen is selected based on the ink properties and the dimensions of the pattern required. Thickness of the printed film is controlled by optimizing printing speed and squeeze angle. After printing, the film is annealed at 120 °C to obtain smooth films with less roughness. The highest efficiency of 0.013% is achieved for the full screen-printed solar cell with the structure Polyethylene terephthalate /Indium tin oxide /Zinc oxide / (P3CT /PCBM/Zinc oxide or P3CT /Zinc oxide /PEDOT: PSS) /silver paste/cold laminated Polyethylene terephthalate film [54]. The annealing temperature and the annealing time are found to be the important parameter in improving the power conversion efficiency of screen printed PEDOT: PSS thin films [54]. The surface roughness and the conductivity of the screen printed PEDOT:PSS film increases with annealing temperature due to the crystallization of the PEDOT:PSS thin films. Comparison between the inkjet printing and the screen-printing process for printing PEDOT: PSS in terms of printing parameters, annealing, sheet resistance, optical transmittance and the efficiency is shown in Table 3.

Table 3
Comparison between inkjet printing and screen printing of PEDOT: PSS [49–54].

Printing process	Important parameters	Annealing method	Conductivity/sheet resistance	Optical transmittance	Thickness	Power conversion efficiency
Inkjet printing	Drop spacing, the surface energy of the substrate, annealing temperature and substrate temperature, [49]	Hot plate oven 120 °C for a duration of 20 min	0.78 S / cm Increased to 152 S/cm by additives EG and EGBE	>90 %	100 nm	3.6 %
Screen printing	Mesh count, annealing temperature and annealing time [54]	Hotplate 120 °C for 10 min	700 to 1100 Ω/□	60 to 70%	250< nm	0.013%

3.2.3. Electron transport layer (ETL)

Electron transport layer (ETL) is a cathode buffer layer in OSCs which acts as an interface between the acceptor and the cathode in inverted geometry. Zinc oxide(ZnO), zinc tin oxide (ZTO), titanium oxides (TiOx), aluminum oxide (Al_2O_3) and niobium pentoxide (Nb_2O_5) are some of the metal oxides which are used as electron transport layer materials in OSCs [55,56]. The main functions of an electron transport layer are: (1) Protection of the photoactive layer from the printed or thermally evaporated cathode (2) abolish the surface states at the exterior of photoactive layer (3) change the energy level alignment by creating dipole moments with cathode or photoactive layer [57].

The most preferred ETL is ZnO because of high transparency (>90%), high electron mobility (> 150 cm^2/Vs), optimum HOMO which enhances the movement of electrons and lower LUMO level, which prevents the movement of holes towards the cathode [58].

The work function of ZnO is intermediate between the acceptor (e.g., PCBM) and the cathode in inverted geometry. It eases the flow of electrons from the photoactive layer to the transparent cathode. Solar cell fabricated with ZnO ETL has better efficiency ~2.3 % than the solar cell fabricated without ETL (0.8%) [59]. For inkjet printing ZnO, the quality of the printed film is affected by ink properties, with different Z (as discussed in Section 2.1) values corresponding to varying concentrations of ZnO. The adhesion of the printed film over ITO substrate can be improved by surface treatments such as Ultra-Violet Ozonization (UVO) treatment. The uniformity of printed film is achieved by varying the substrate temperature during printing. Further, the annealing temperature of the printed film affects the final printed film morphology. For ZnO, film annealed at 175 °C is found to be smoother than the one annealed at 250 °C [60]. Surface scattering is less in smoother film which improved the transmittance of ZnO annealed at 175 °C. The thickness of the printed films also played an important role in device performance. The thickness of ZnO film can be modified in two ways: (1) by changing the drop spacings or (2) by printing multiple layers of ink. When the drop spacing is reduced by half, the thickness of the film is roughly increased by double.

The efficiency of an organic solar cell with a thin layer (25 nm) of ZnO is higher (3.2%) than the devices with the thicker (45 nm) ZnO film (2.7%) [60]. It is possibly because of high fill factor and short-circuit current for devices with thinner zinc oxide film (25 nm) as in thinner films more number of photons can pass through and also surface roughness is less in the thinner film which results in better contact between ZnO film and the photoactive layer [60].

It is also mentioned in some research works with the structure ITO/PEDOT:PSS/ZnO/photoactive layer/MoO_3/Ag that the device performance is independent of thickness when ZnO is printed over ITO. But when printed over PEDOT: PSS the thickness plays a significant role and should be in the range of 20–60 nm for better device performance [61]. This is because minimum thickness of ZnO is required to fully cover the PEDOT:PSS layer. The power conversion efficiency of the inkjet printed devices is 17% more than the spin-coated devices. The comparison is also made between the devices fabricated by spin coating, thermal evaporation and inkjet printing for organic solar cells with geometry Glass/ITO/ZnO/PTB7-Th:PCBM/V_2O_5/Ag. The higher efficiency of 9.42% is achieved for the spin-coated ZnO devices, followed by thermal evaporation (8.17%) and the last inkjet printing (7.47%). This is due to the reduced photon absorption (60%) for devices with inkjet printed ZnO in the range of 300–600 nm. Also, the short current density of inkjet printed devices was less (14.85 $mAcm^{-2}$) than the spin-coated (18.62) and the thermal evaporated devices (16.94). All the ZnO films fabricated by different methods show varying surface morphologies as examined in AFM images shown in Fig. 6. Thermally evaporated films show granular structures, spin-coated ones have mountain and valley like structures and inkjet printed films show formation of aggregates [62].

For screen printed ZnO, the ZnO films were first dried at 110 °C for two hours to reduce the solvent partially and further annealed in ambient conditions in furnace at 550 °C for 10 min to stabilize the film and to burn the organic materials. Thickness of the screen-printed films is high, generally in the micron metre range. The crystalline films of screen printed ZnO show grain size of around 25 nm as estimated from sharp XRD peaks using Debye

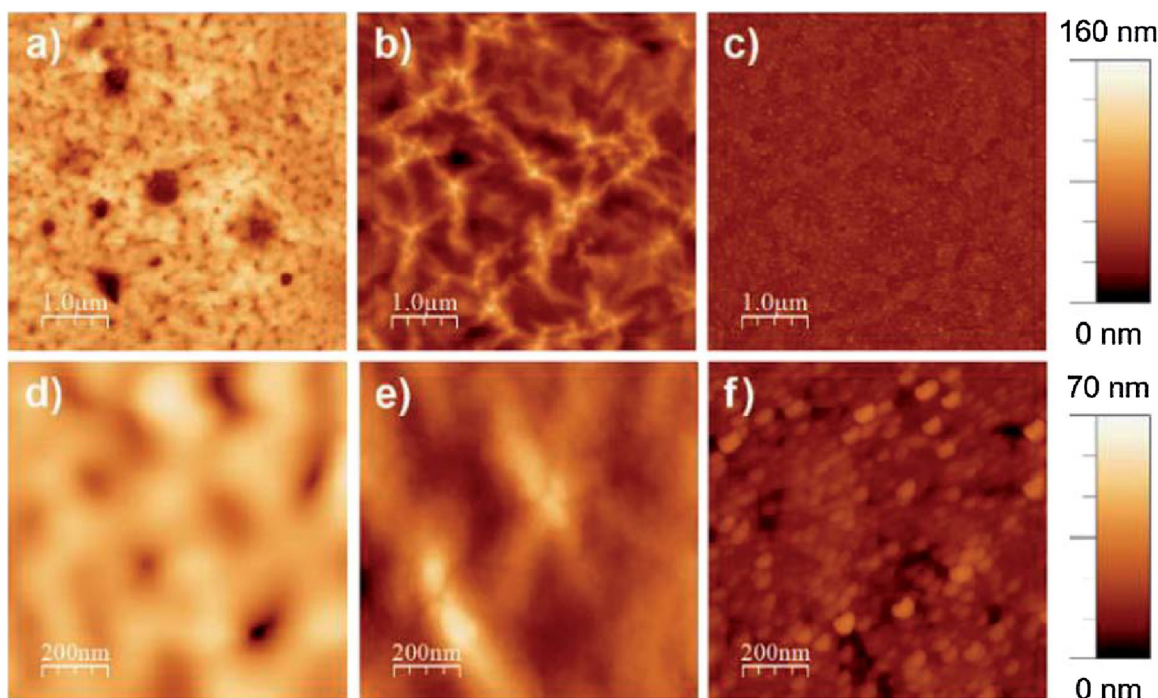**Fig. 6.** 5 X 5 μm AFM image of (a) inkjet printed zinc oxide (b)spin coated zinc oxide (c) thermally evaporated Zinc oxide 1 X 1 μm AFM image of (d) inkjet printed Zinc oxide (e) spin coated zinc oxide and (f) thermally evaporated Zinc oxide [62].

Table 4
Comparison for printing zinc oxide between inkjet printing and screen-printing processes. [60–65].

Printing process	Important parameters	Annealing method	Conductivity/sheet resistance	Optical transmittance	thickness	Power conversion efficiency
Inkjet printing	Concentration Z number, annealing temperature, thickness (60), drop spacing (61)	Hot plate oven 175 °C for 10 min		85 %	25 – 45 nm	3.5 % for P3HT: PC$_{61}$BM based devices. 7.47 % for PTB7th: PCBM based devices.
Screen printing	Annealing temperature, the film thickness (62)	Hotplate 30 °C for 60 min and 550 °C for 10 min in a muffle furnace.	Sheet resistance 300 Ω/□). After doping with aluminum, it was reduced to 10 Ω/□).	80 %	1 μm	

Scherrer's formula [63]. The electrical resistivity of printed ZnO is high (10.5×10^{-2} Ωcm) and it can be reduced by doping with Aluminium.

The screen-printing paste was prepared by the addition of zinc chloride and ethylene glycol to the zinc oxide powder and the viscosity of the paste was adjusted by paraffin [64]. The film adhered to the base substrate after the removal of the solvents. The volatile organic solvents were partially removed, and the film adhered to the base substrate. The film thickness was 10 μm for both undoped and doped samples. XRD of undoped ZnO showed a polycrystalline structure. The screen-printed ZnO thick films had the same crystalline structure as that of the ZnO powder [65]. Comparison between the inkjet printing and the screen printing process for printing ZnO in terms of printing parameters, annealing, sheet resistance, optical transmittance and the efficiency is shown in Table 4.

3.2.4. Photoactive layer

The process of conversion of light energy into electrical energy takes place in the photoactive layer. The absorption coefficient of organic semiconductors is high (100000/cm) in comparison to their inorganic counterparts [66]. Thin film plastic substrates such as PET can be utilized to produce OSCs because of high absorption coefficient. As the light falls on an OSC, excitons (electron-hole pair) are formed in the photoactive layer. These excitons move towards the interface of acceptor and donor by diffusion and get separated into electrons and holes at the interface due to the difference in energy level between the HOMO of the donor and the HOMO of the acceptor. Finally, the generated electrons and holes move to the respective electrodes [67].

The printing of the photoactive layer is a challenging one as the material is sensitive to oxygen and moisture present in the outside atmosphere. The printing must be performed with in a short duration to prevent the degradation of the photoactive layer or the printing must be carried out in nitrogen or argon inert atmosphere. Also, the chlorinated solvents such as oDCB used in the printing of organic solar cells are harmful to health. This problem is solved to some extent by using nonhalogenated solvents such as toluene.

The most widely used electron donor material for printing is P3HT because of its very high stability and low cost and the widely used electron acceptor material is fullerene PC$_{60}$BM [68]. The first inkjet-printed active layer was P3HT:C60 printed over PEDOT:PSS in a normal geometry(Glass/Indium tin oxide /PEDOT:PSS/P3HT:C60Lithium fluoride /Aluminium) using a micro-fab inkjet printer on print on fly mode where the drop of ink is dispensed when the stages are at the move. The efficiency achieved was very less 0.0003% due to the crystallization of C60 film [69]. The crystallization of C60 is due to the low solubility of C60 on ODCB also the penetration of the solvent molecules into the C60 crystal lattice and distort its structure [70].

Ortho-dichlorobenzene (oDCB), which is the most preferred solvent for the production of OSCs using spin coating of P3HT:PCBM, cannot be used as a standalone solvent for inkjet printing [71]. Since the surface tension of oDCB is high (39 mN/m) a non-uniform film with thickness variation is produced by inkjet printing. Therefore, a combination of a high boiling solvent such as oDCB (180 °C) and a low boiling solvent such as mesitylene (164 °C) is used for the printing of photoactive layer [66]. The high boiling solvent prevents the nozzle clogging and the low boiling solvent improves the spreading of ink. Inkjet printing of P3HT: PCBM blend dispersed in oDCB (68%) and mesitylene (32%) solvent mixture resulted in an efficiency of 3 % due to the better morphology [71].

Apart from the solvent combination, the regio-regularity of the P3HT also plays an important role in inkjet printability [72]. Regioregularity is the arrangement of 3-substituted thiophenes in three different ways when two monomers are linked to each other in second and third position. The possible arrangements are head to head, tail to tail, and head to tail. The conductivity of regiorandom is less than the conductivity of regio regular. In inkjet printing, it was found that the 98% regio-regular P3HT is not suitable because the shelf life of the ink is affected due to the formation of aggregates. The best suitable regio-regular percentage for inkjet printing is 96% and it resulted in an efficiency of 3.5% [72].

The molecular weight of the donor also found to play a critical role in the efficiency of bulk heterojunction organic solar cells. The higher efficiency of 2.5% was achieved for the P3HT: PCBM based organic solar cells when the molecular weight of P3HT was greater than 10 Kg/mol. This is due to the improved charge carrier(hole) mobility and proper intermolecular ordering of the P3HT [73]. Similar results are observed in PTB7: PCBM based bulk heterojunction OSCs. When the molecular weight of the donor PTB7 was increased from 18 to 128 kg/mol, the efficiency was found to increase from 5.41% to 8.50%. The improvement in efficiency with molecular weight was mainly due to the enhanced optical absorption, increased charge carrier mobility and appropriate phase separation in the PTB7:PC$_{71}$BM interpenetrating networks in the bulk heterojunction [74]. Hence, the molecular mass of the donor material has to take into consideration while formulating the photoactive layer ink.

Devices based on P3HT: PCBM needs annealing (usually at at 150 °C) after printing for better morphology as P3HT is semi-crystalline in nature. Post thermal treatments such as annealing cause additional energy consumption during the roll to roll production of OSCs. Hence it is not desirable. So, Alexander Lange inkjet printed PFDTBTP poly(9,9-dioctylfluorenyl-2, 7-dyil–CO-{10,12-bis(thiophen-2-y)-3,6-dioooctyll-11-thia-9,13-diaza-cyclopentatriphenylene} a novel amorphous polymer using a Dimatix inkjet printer [75]. For amorphous polymer PFDTBTP, high-temperature annealing is not required. Also, because of the presence of alkane side chains in the structure of PFDTBTP, it is soluble in many solvents such as chlorobenzene, trichlorobenzene, anisole and tetral. The devices are fabricated with chlorinated solvents such as chlorobenzene/trichlorobenzene and unchlorinated solvents such as (anisole/tetralin) solvent systems. The
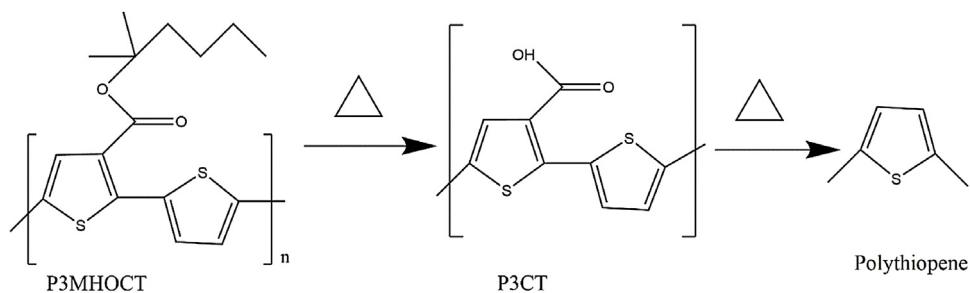
Fig. 7. P3MHOCT was converted to P3CT first and then P3CT was converted to polythiophene during thermoclevage [84].

highest PCE of the devices fabricated with chlorinated solvents is 3.5% and the PCE of the non-chlorinated solvents devices is 2.8% [76]. The fill factor and short circuit current density are high for the active layer with chlorinated solvents because of better morphology. P3HT:PCBM blend is also prepared with non-chlorinated solvent mixture tetraline, Indan and O-xylene (1:1:1) with 1.3% weight concentration of both PCBM and P3HT. An efficiency of 2.2% is attained for solar cells produced with spin coating and an efficiency of 2.09% is attained for solar cells produced by inkjet printing. When the devices are fabricated over Mo/Al/Mo grids, the efficiency is reduced to 1.78% [77].

PCDTBT poly[N-9'-heptadecanyl-2,7-carbazole-alt-5,5-(4',7'-di -2-thienyl-2',1',3'-benzothiadiazole)] is another donor polymer which is used in the inkjet printing of organic solar cells [78]. PCDTBT is a donor-acceptor copolymer with electron donating carbazole units and electron accepting 1,2,3-benzothiadiazole. To understand the role of solvent mixtures on device performance, three-layered solar cells (PEDOT:PSS/PCDTBT/Al) are fabricated. Devices made up of Chlorobenzene (CB) and Chlorobenzene: Chloroform(CF) (1:1) exhibited a device performance of 3%. With devices based on Chlorobenzene: Mesitylene (MT) (1:1) efficiency of 4% is achieved. The solvent combination of CB:MT:CF leads to a uniform photoactive layer film resulting in an efficiency of 5.05% [78].

P3HT:PCBM is screen printed using a mesh count of 181/cm. The important parameters for screen printing the active layer are squeeze pressure, squeeze speed and the gap between the substrate and the screen. Chlorobenzene is used as the solvent for preparing the P3HT:PCBM blend. The height and the surface roughness of the screen printed layer are 40 nm and 2.3 nm respectively. The efficiency of the device measured under the light of wavelength 488 nm is 4.3% [79]. In this work, a diode laser of wavelength 488 nm is used for illumination. The efficiency of P3HT:PCBM based OSC measured under monochromatic illumination (488 nm) is higher than that under 1 sun illumination as more number of photons are absorbed in 488 nm monochromatic illumination where the optical absorption of the material P3HT is at peak.

The active layer blend solution consisting of MDMO-PPV: PCBM dissolved in chlorobenzene is screen printed using a 420-mesh screen. Annealing is performed after printing at 50 °C for a time duration of 10 min. The power conversion efficiency of the devices with the geometry Glass/ITO /PEDOT:PSS/MDMO/PPV/PCBM blend/Aluminum is in the range of 2–3% [80]. Similarly, MEH-PPV:PCBM blend is screen printed with a squeegee made up of polyurethane set a squeegee angle of 45∘ on ITO coated glass substrates in ambient conditions. The active area of the cell is 4.5 cm². The screen-printed active layer film is non-homogenous when printed at very low speed, whereas high speed printing provides uniformity. Moreover, the final thickness of the film was found to increase with high squeegee pressure. This is because more volume of ink is passed through the screen with high squeegee pressure. The efficiency of the solar cell fabricated with screen

printed MEH-PPV: PCBM based solar cell is found to be 0.65% [81]. MEH-PPV was printed on the PET substrate using a silk screen with a mesh count between 140 and 220 cm⁻¹ and thread diameter 27 μm. The effect of molecular weights of MEH-PPV was observed on the rheological properties of the ink, where the ink with mean molecular weight [82], shows Newtonian behavior whereas the one with high molecular weight, showed non-Newtonian behavior, specifically required for screen printing. Further, it also affects the required printing conditions and hence thickness of the final printed film.

The MEH-PPV ink is prepared by dissolving in chlorobenzene (concentration 14.6 mg ml⁻¹) to get a solution of viscosity 70 mPa S. The C_{60} layer of thickness 220 nm and an aluminium electrode of thickness 34 nm are thermally deposited over the photoactive layer and the solar cell is laminated in an office laminator using an aluminium foil at the temperature of 125 °C. The cells are connected in series and the PCE is found to be 0.0046% [83].

The viscosity of the ink should be high for applications in screen printing. But the viscosity of the photo active layer blend solutions such as P3HT:PCBM is very low (10 mPa S). The printing of such a low viscous solution is impossible and the solution just passes through the mesh on the screen. Since the ink is printed in ambient conditions, the solvent evaporation rate is high and the solute particles are deposited on the screen mask [84]. To overcome this problem, thermoclevage solvents are used. Thermoclevage solvents are solvents with high viscosity and low drying time [84]. This property of thermoclevage solvents helps in printing the conjugated polymers such as P3HT. After printing, the solvent is removed by heating in an oven. The polymer P3MHOCT (poly-(3-2-methylhexyloxycarbonyl) dithiopene) is screen printed and the aliphatic chains are removed during annealing at 140 °C for four hours to form polythiopene [84]. The chemical reaction for the same is shown in Fig. 7. The donor P3MHOCT and the acceptor ZnO are mixed in a blend and the structure of the device is Polyethylene terephthalate / Indium tin oxide / Zinc oxide / P3CTZnO / PEDOT:PSS /silver -paste / PET lamination [84]. Five solar cells are connected in series in the concentric ring form and the active area of the cell is 75 cm². The short circuit current of the cell is −1.53 mA, open circuit voltage is 2.64 V, fill factor is 2.26% and the maximum power is 1.04 mW. All the layers are screen printed (PEDOT:PSS, ITO and the photoactive layer) and the images are shown in Fig. 8.

Comparison between the inkjet printing and the screen-printing process for printing indium tin oxide in terms of printing parameters, annealing, sheet resistance, optical transmittance and the efficiency is shown in Table 5.

3.2.5. Conductive electrode inks

The last layer in the OSCs is the back metallic electrode. The metal electrode is also used as the front electrode (grids) in the case of ITO free OSCs. Among the metal electrodes, silver is widely used because of its resistance to oxidation. Some of the other materials which are used as electrodes are gold, copper and graphene.
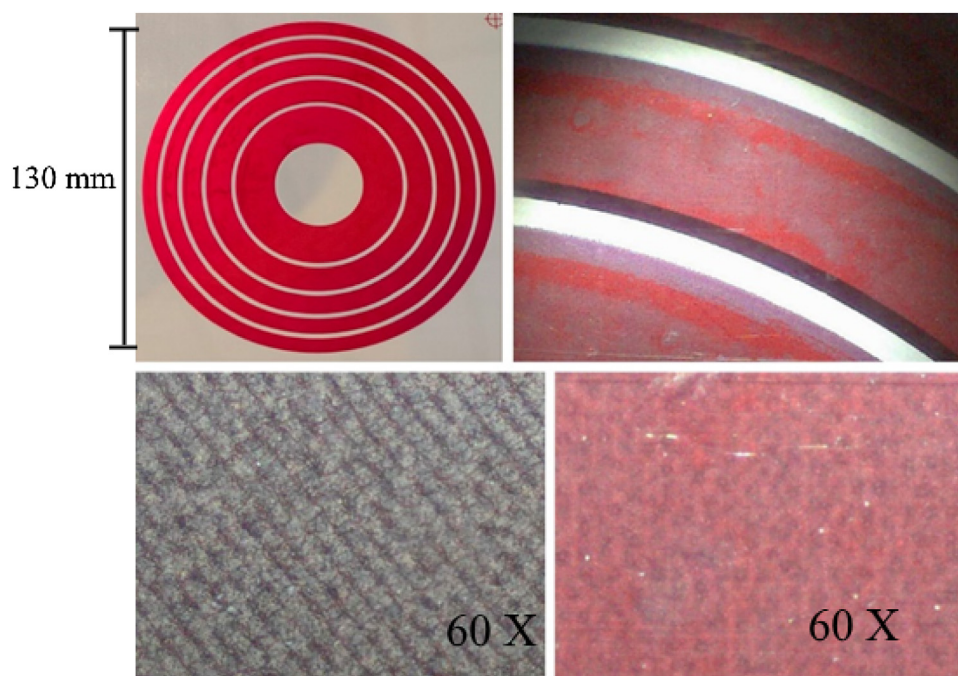
Fig. 8. Uniform wet print of the screen printed photo active layer (top left) Microscopic image showing non-uniformity of the photoactive layer due to dewetting and the underneath ZnO layer (top right), Improper print with mesh structure reproduced at a magnification of 60 (bottom left) and a better print with out mesh structure at a magnification of 60 (bottom right) [54].

Table 5
Comparison between inkjet printing and screen printing for the printing of photoactive layer [68–84].

Printing process	Important parameters	Annealing method	Solvents	Surface roughness	Thickness	Power conversion efficiency
Inkjet printing	Drop spacing, the boiling point of the solvent [71], regio regularity [72] and, annealing temperature [72]	For semi crystalline polymer such as P3HT Hot plate oven 150 °C degree C for 10 min	Combination of solvents such as oDCB and mesitylene is used to prevent nozzle clogging and improve wetting.	∼ 1 nm	30 to 90 nm	3.5 % for P3HT:PC$_{61}$BM based devices.7.47 % for PTB7th: PCBM based devices.PCDTBT 5.05 %.
Screen printing	Squeegee shape, the gap between the screen and the substrate, Squeegee type, squeegee angles, printing speed, squeegee pressure [79], thread diameter, mesh count [80] and viscosity of ink [81]	Hotplate at 30 °C for 60 min and 550 °C for a time duration of 10 min in a muffle furnace.	A single solvent such as chlorobenzene was used. To improve viscosity thermoclevage solvents are used.	∼ 2 nm	40 to 120 nm	MDMOPPV: PCBM 2 to 3 %. MEH: PPV: PCBM 0.65 % P3HT: PCBM 4.3 % (illumination 488 nm)

3.2.5.1. Optimization of process conditions for inkjet printing of electrodes. The optimizing parameters for inkjet printing can be classified into waveform parameters, printer parameters and the sintering parameters. The wave form parameters voltage, time and frequency control the ejection of the droplet from the print head nozzle [85]. The waveform parameters decide whether the ejected droplet is a single droplet or a satellite drop. The waveform parameters also control the velocity of the droplet and the drop volume [86].The printer parameters which influences the width and the uniformity of the printed line are drop spacing, substrate temperature and the number of printing layers [87]. When the drop spacing is more, there will be no contact between the drops resulting in isolated drops. If the drop spacing is reduced, the isolated drops merge but retain the circular profile of the drop resulting in scalloped pattern. If the drop spacing is reduced further, a smooth uniform line

is formed [15]. Figure 9(a) shows the effect of drop spacing and annealing temperature on the inkjet printing of PEDOT: PSS. The thickness of the inkjet printed film was high at low drop spacing due to the larger overlap of the two drops [49]. The drop spacing is optimum between 30 μm and 32 μm [49]. The annealing of the ink was performed at two different temperatures (100 °C and 120 °C). The lower roughness value of 4.0 nm was achieved at the temperature of 120 °C [49]. The next important printer parameter is substrate temperature. The increase in surface temperature leads to the suppression in the spreading of the ink which in turn leads to the reduction in drop diameter at higher temperatures. The diameter of the drop and the height of the drop is calculated from the measured contact angle using expression 2 and 3 and compared with the experimental results [88]. The drop diameter was found to decrease with the increase in surface temperature due to
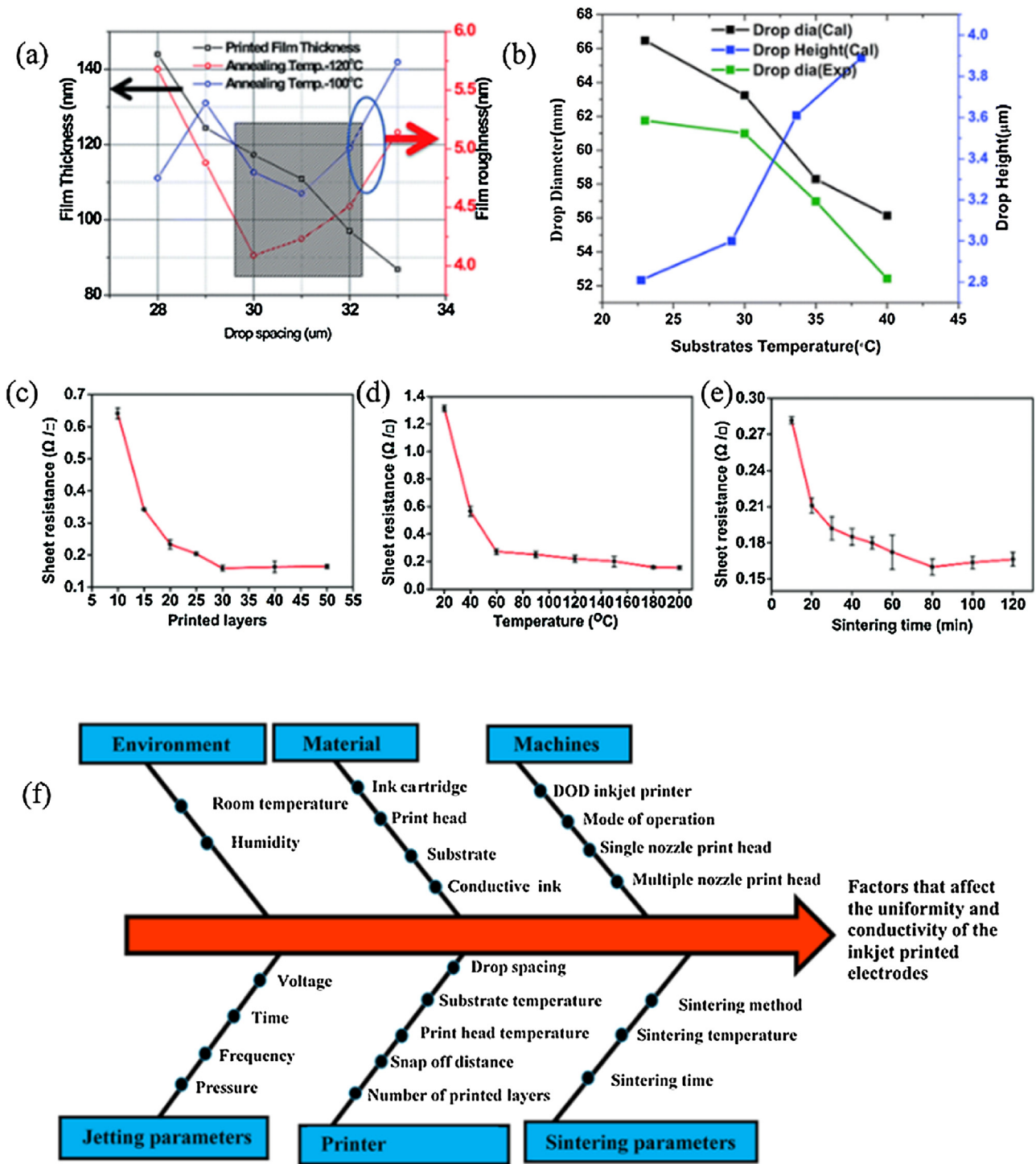
Fig. 9. (a) shows the influence of drop spacing on the inkjet printed thin film thickness and roughnesss [49] (b). Shows the effect of substrate temperature on the diameter and the height of the drop [49](c) relation between sheet resistance of the inkjet printed thin film and the number of printed layers (sintering temp: 180°C,time 80 min) [89] (d) relation between sheet resistance and the sintering temperature (number of layers 30, time 80 min) [89] (e) relation between the sheet resistance and the sintering time(number of layers 30, temp 180°C) [89] and (f).Parameters and environmental conditions which determine the qualited of the inkjet printed line.

the evaporation of the solvent as shown in Fig. 9(b). The surface temperature also enhances the coffee ring formation due to the increased evaporation rate at the three-phase interface.

$$D = d_0 \sin\theta \left\{ \frac{1}{(3 - 2\sin^2(\frac{\theta}{2})\sin^4(\frac{\theta}{2})} \right\}^{1/3} \tag{2}$$

$$H = d_0 \sin^2\left(\frac{\theta}{2}\right) \left\{ \frac{1}{(3 - 2\sin\left(\frac{\theta}{2}\right))\sin^4\frac{\theta}{2}} \right\}^{1/3} \tag{3}$$

Another important variable to increase the height of the printed line is the number of printed layers. The sheet resistance of the printed line decreases exponentially with the number of printing layers as shown in Fig. 9(c). The sintering of the printed line must be performed before printing each layer to increase the line height.
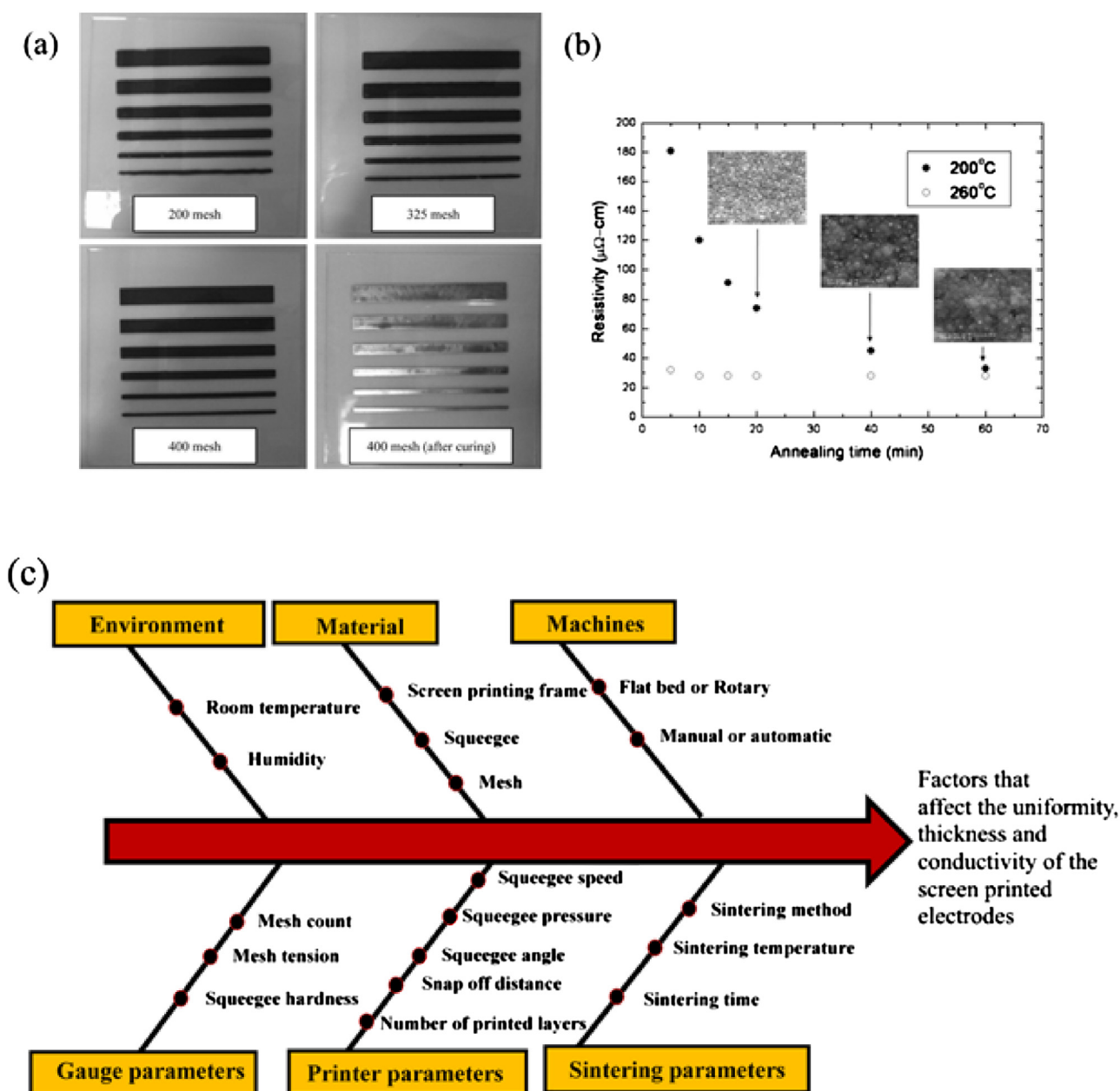
Fig. 10. (a) Images of screen-printed ink with 200, 325 and 400 mesh count screens are shown in the first three pictures. In the last picture image after heat treatment at 200 °C for 5 min is shown [90]. (b) Relation between electrical resistivity and annealing time for two different temperatures (200 °C and 260 °C) (c) Factors which affect the uniformity, thickness and conductivity of the screen-printed electrodes.

Otherwise there will be only increase in width of the line due to the spreading of the ink. Sintering temperature and time also play an important role in the electrical and the morphological characteristics of the inkjet printed layer. Figure 9(d) shows the reduction of the sheet resistance value of the inkjet printed silver track to 0.22 $\Omega/\square$ after annealing at 120 °C. from 1.31 $\Omega/\square$ at room temperature [89]. Similarly, the sheet resistance was found to decrease gradually with sintering time and was stable after 80 min [89] as shown in Fig. 11(e). The influence various parameters and the process conditions on the inkjet printing of conductive ink is shown in Fig. 11(f).

3.2.5.2. Optimization of process conditions for screen printing of electrodes. The optimization parameters for screen printing are mesh count, squeegee speed, squeegee pressure, mesh tension, squeegee hardness, squeegee blade, squeegee angle, snap off distance and number of printed layers. The effect of mesh count on the quality of the screen printed lines of width (0.5,1.5,2.5,4.5 and 5.5 mm) [90] are shown in Fig. 10(a). Mesh count is the number of openings in the screen per square inch. The sharpness of the screen-printed lines was found to improve with the mesh count. When the screen printing was performed using screens of three different mesh counts (200,325 and 400) and a polyurethane squeegee, the lines printed with 400 mesh count are found to be sharper than the other two [91]. The squeegee speed which is the optimum speed of the movement of the squeegee for uniform printing is dependent on many factors such as viscosity of the ink, screen tension and mesh count. The squeegee speed should be low for high viscous inks [91]. If not unwanted pattern of the screen will show in the print. The squeegee speed should be high for high tension screen as the screen acts as like a cheese grater for a high-tension screen, allowing the ink to readily pass through. The squeegee speed should be
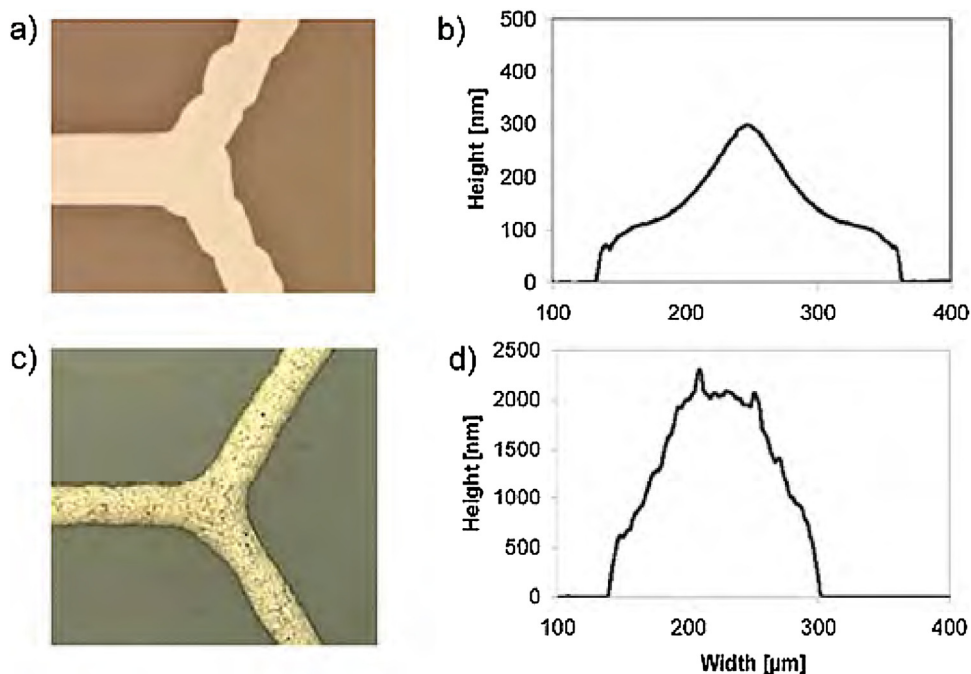
Fig. 11. (a)inkjet printing (b) screen printing [106].
(a) optical image of the inkjet printed silver grid on PEN film at a magnification of 50 (b) Profile of the inkjet printed silver line (c) optical image of the screen printed silver grid on PEN film at a magnification of 50 (d) profile of the screen printed silver line.

low for low tension screens as the screen acts like a filter and ink should be forced through the screen with high squeegee pressure and low squeegee speed. The squeegee speed also affects the thickness of the deposited film. Faster squeegee speed result in a thinner film and slower squeegee speed result in a thicker film [92]. This is because during faster squeegee speed, the ink has less time to penetrate through the screen and transfer to the substrate. Squeegee hardness, squeegee shape and squeegee angle are the important parameters of the squeegee. The shore which is the unit for squeegee hardness should be high for a high-resolution pattern. So that, higher pressure with low deformation of the squeegee results during the printing process [92]. The profile of a rectangular squeeze is in the form of a narrow contact line while a rounded squeegee results in a broader contact line resulting in higher volume of ink transfer [93]. A high mesh count and higher hardness squeegee is required for printing grids and back electrodes. The squeegee blade angle should not be too low or too high. If the squeegee blade angle is high, large volume of ink pass through the screen. When the squeegee angle is low, ink will not penetrate through the screen [94]. The snap off distance which is the distance between the screen and the substrate depends on the frame dimension, the size of the image, screen tension and composition of the ink [95]. Apart from the screen-printing parameters other parameters such as the number of printed layers3, sintering temperature and sintering time also play an important role in the screen printing of conductive inks. The sheet resistance of the screen-printed pattern is reduced as the thickness of the printed film increases with the number of printed layers. The sintering temperature and time also play an important role in the conductivity of the screen-printed line. Figure 10(b) shows screen-printed conductive lines sintered at two temperatures (200 °C and 260 °C). In the case of screen-printed silver line annealed at 200 °C the resistivity was initially high (180 μm/cm after 5 min) and gradually decreases with time and reaches the lowest value after 60 min [96]. In the case of screen-printed silver line annealed at 260 °C, the resistivity reaches the lower value (30 μm/cm) after 5 min immediately. After that it gradually decreases up to 10 min and remains constant afterwards

[96]. Figure 10(c) shows the factors which affect the uniformity, thickness and conductivity of the screen-printed electrodes.

3.2.5.3. Conductive inks as front electrodes. The transparent electrode ITO is costlier since Indium is a rare metal and ITO is brittle, making it an unpreferable candidate for flexible electronics. Hence alternative materials like graphene [97], carbon nanotubes [98,99], high conductive PEDOT: PSS [100] and silver nanowires [101] have been explored as transparent electrodes. PEDOT: PSS is used as an alternative for ITO. But PEDOT: PSS has disadvantages such as high sheet resistance (200–500 Ω/□) and low transmittance (70–80 %) [102]. To scale down the sheet resistance of PEDOT: PSS, silver grids is used as the current collection electrodes The grids are initially fabricated by diffusion transfer reversal technique [102] and then by screen printing a nano silver paste with a 55% silver content using a DEK screen printer [103]. The silver paste comprises silver nanoparticles and a soluble silver complex. The height of the silver grid is 1 μm and hence the PEDOT: PSS cannot be spin coated above the silver grids. The silver grids are embedded into the barrier layer to solve this problem. Grids with both line patterns and honey comb patterns are printed. The power conversion efficiency of devices fabricated over ITO, honey comb grids and line pattern grids are 0.95, 1.82 and 1.93 respectively. Then the grids are inkjet printed with different line spacings (20,106,753.3,2.5,2 and 1 mm). The maximum efficiency of 1.46% is attained for a pitch size of 2.5 mm.

The current increases initially with the addition of more grid lines and is maximum at the grid spacing of 5 mm after that there is a decrease in current due to the shadowing effect. The decrease in efficiency is mainly due to the blocking of light by the silver grids [103]. The height of the grid cannot be increased beyond a limit because of the problem in coverage of grids by PEDOT: PSS. To overcome this problem the grids are embedded into the substrate by imprinting thermally and then filled with silver. During thermal imprinting, a nickel master grid is mounted on a roller (steel). The PET foil is passed between the nickel grid (heated to 110 °C) and the backing steel roller. The pattern in the grid is transferred to the
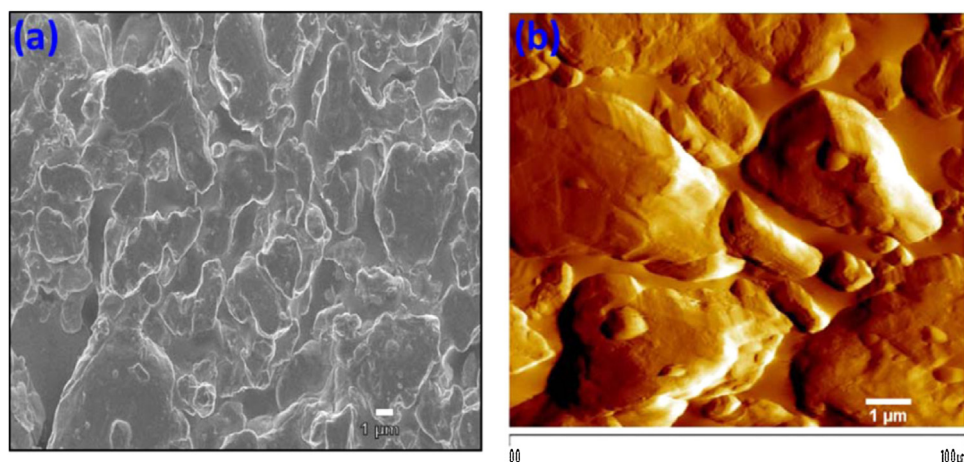
Fig. 12. (a) FESEM image and (b) AFM image of screen printed silver back electrode [111].

Table 6
Comparison between screen and inkjet for printing conductive inks [54,102–111].

Printing process	Important parameters	Annealing method	sheet resistance	Optical transmittance	Line width and height	Power conversion efficiency
Inkjet printing	substrate temperature, drop spacing the surface energy of the substrate and the annealing temperature.	Hot plate oven 200 °C for 2 hours	15 Ω/□	80 %	Width 130 to 150 μm and height 200 to 300 nm.	2.3 % (grids) 0.83 % (back electrode)
Screen printing	Mesh dimension, squeegee pressure and squeegee, snap off distance and annealing temperature	Hot plate oven 200 °C for 2 hours.	1 Ω/□	70 to 75 %	160 μm and 2 μm.	ITO- 0.95 % Ag honeycomb /HC PEDOT: PSS 1.82 % Ag lines/HC-PEDOT 1.93 %. 2.1% (Flatbed screen back electrode) 1.79% (rotary screen back electrode)

PET foil and the pattern is filled with silver ink. The fill factor of the embedded silver grids is more than the ITO coated glass, but the short circuit current density is less because of shadow loses. The embedded grids have the advantages of the very smooth profile of the substrate and less shadow loss compared to printed grids. But the manufacturing process involves two distinct steps: thermal imprinting and filling [104].

A comparison is made between grids printed by flexography and inkjet printing process. An efficiency of 0.75% is achieved for inkjet printed silver grid and an efficiency of 1.82% is achieved for flexoprinted grid [105]. The fill factor of the devices made up of inkjet printed grids are less when compared with the flexoprinted grids. This is due to the higher sheet resistance of the inkjet printed grids (60 Ω/□) than flexoprinted grids (10 Ω/□) [105].

Figure 11(a) and 11(b) shows the microscopic image of inkjet printed and the screen grid pattern, respectively. Scalloping effect can be observed in inkjet printing due to the improper drop spacing. The thickness of the inkjet printed line is less (approx. 300 nm) and the thickness of the screen-printed line is high (around 2000 nm) [106].

3.2.5.4. Conductive inks as back electrodes. Printing of back electrode is not easy as annealing cannot be performed at high temperature. Also, the solvents used in the conductive ink penetrates the underlying organic layers and reduces the device performance and stability. The nanoparticles used in the conductive ink can pierce into the photoactive layer which is thin and fragile. ZnO is used as an intermediate layer between the active layer and back electrode silver to solve this problem [107]. The effect of annealing on the zinc oxide layer is tested for two dif-

ferent temperatures 100 °C and 150 °C. A highest efficiency of 0.21% is achieved at a temperature of 150 °C because of better morphology. Some of the other solution processable buffer layers which serve as solution processable electron transport layer are titaniumdioxide(TiO_2), tin oxide(SnO_x), cerium oxide (CeOx) and metal-acetylacetonate chelates [44]. Zirconium acetylacetonate (ZrA-cac), Titanium(IV)oxide bis(2,4-pentanedionate) (TOPD) and Titanium (diisopropoxide) bis (2,4-pentanedionate) (TIPD) are some of the chelates which can be directly used as a buffer layer without converting into metal oxide [108]. A novel water/alcohol soluble conjugated polyfluorene polyelectrolyte (PFNR2)poly[(9,9-bis (3′-(N,N-dimethylamino)propyl)-2,7-fluorene)-alt-2,7-(9,9-dioctyl fluorene)] which acts as the highly efficient electron injection layer between the light emitting polymers and high work function metals in light emitting diode can also be used as electron transport layer in OSCs between the silver back electrode and the photoactive layer [109].

When comparison is made between the rotary screen printing, inkjet printing process, flatbed screen printing and the flexography printing for printing the back electrode, it is found that the flat bed screen printing is the best process for back electrode. ALTRAUN Technik flatbed screen printer is used for printing the silver paste with a 120 wires per inch screen and annealing was performed at a temperature of 140 °C for 2 min. The power conversion efficiency achieved for flexo printing, inkjet printing, rotary screen printing and flat bed screen printing are 0.55%, 0.83 %, 1.79% and 2.1%, respectively. The high efficiency of the screen-printed back electrodes are due to fill factors close to 50%. The fill factors of the inkjet and flexo printed solar cells are only 31%. The thickness of the rotary screen-printed films is about 3–500 μm and the flat bed

Table 7
List of screen printed OSCs with all the important parameters for device fabrication and characterization.

S.No	Device structure and geometry	Screen printer and printing parameters	Screen printed layers	Annealing temperature in °C and thickness in nm	Active area	PCE %	Additional information
1.	PET/Indium tin oxide /Zinc oxide / (P3CT/PCBM/Zinc oxide or P3CT/ZnO)/ PEDOT:PSS/silver (inverted) [54]	ZnO ink Viscosity of the solution 20.4 mPaS at 24 °C. P3MHOCT/ ZnO ink viscosity 39.3 mPaS	Zinc oxide (180) PEDOT:PSS (165 mesh screen), photoactive layer (180 mesh screen) Silver (120 mesh screen)	ZnO (140 °C for 4 hours.) PEDOT: PSS (120° for 15 min), Active layer (4 h at 140 °C)	75 cm^2	0.013 %	
2.	Glass/ITO/PEDOT: PSS/MDMO-PPV: PC$_{61}$BM/Al (Normal) [79]	Manual screen printer Thread diameter 30 μm, mesh count 181/cm, standoff distance of a few mm	MDMO PPV PC$_{61}$BM	40 nm		4.3	Roughness 2.6 nm
3.	Glass/substrates/ ITO/PEDOT: PSS/MDMO-PPV-PCBM blend/Al [80]	420 mesh screen Squeeze pressure, squeeze speed, squeeze shape, squeeze angle, and the gap between screen and the substrate	Active layer MDMO PPV: PCBM	50 °C for 15 min Thickness 100 nm	6 mm^2	2.3 %	
4.	Glass/Indium tin oxide /PEDOT:PSS/ MEH-PPV:PCBM/Lithium fluoride /Aluminum (Normal) [81]	ESSEMTEC screen printer with polyurethane squeegee set at an angle 45° and shore hardness 85. Squeegee pressure, speed of the squeegee movement, mesh size and snap off distance.	MEHPPV: PCBM	125 to 150 nm (depends on the squeegee pressure)	20.25 cm^2	0.65 %	
5.	PET/ITO/silver/ MEH-PPV/C60/Ca/Al/PET (Normal) [83]	Viscosity (70 mPa S) and mesh count (140 to 220 cm^{-1})	Etch resist, silver epoxy contacts and MEH-PPV	140 to 150 nm		0.046 %	
6.	PET/silver grid/HC PEDOT: PSS/MEH-PPV: PCBM /Al [103]	NA	HC PEDOT	1 μm	1.2 cm^2	JSc = 1.8 × 10^{-3}A Voc =750 mV.	Sheet resistance HC PEDOT: PSS 1k Ω/□ reduced to 400 Ω/□ after an underlay of silver grid.
7.	PEN/Barrier/Ag grid/HC PEDOT/OPV/LiF /Al/Barrier [104]	Dek Horizon screen printer	Silver grids	Line width 160μm Height of the grid 2μm	4 cm^2	0.95 % (ITO) 1.82 % honey-comb grid) 1.93 % (silver lines grid)	The sheet resistance of the printed grid 1 Ω/□.
8.	PET /silver / PEDOT:PSS / ZnO /P3HT:PCBM/Ag [110]	Flatbed screen printer ALTRAUN Technik GmbH (120 mesh screen) Rotary screen printer (215 mesh nickel screen)	PEDOT: PSS rotary screen printed, Silver back electrode (screen printing, flexo printing and inkjet printing)	Hot air (140 °C and infrared dryers) FBSP Ag thickness 8 μm RSP Ag thickness 10 μm.		2.1 % (FBSP) 1.79 % (RSP)	Sheet resistance FBSP 67 m Ω/□. RSP 47 m Ω/□.

No.	Configuration	Parameters	Electrode	Annealing	Area	Efficiency	Remarks
9.	Glass/Indium tin oxide/Zinc oxide / P3HT:PCBM/ PEDOT:PSS/silver [111]	Squeegee speed, squeegee pressure and viscosity of the ink.	Silver back electrode	150 °C for 10 min.15 μm.		2.58 %	The sheet resistance of the screen printed silver 0.06 Ω/□ Surface roughness 178 nm
10.	Indium tin oxide / MEH-PPV/ C60/Aluminium (Normal) [112]	AT 701 (ALRAUN TECHNIK) Mesh count, screen tension, distance between the screen and the substrate, squeegee angle, squeegee hardness, squeegee edge, temperature, humidity and airflow around the printing area.	Photo resist and silver paste		7.2 cm^2	10^{-5} 2 × 10^{-4}	91 solar cells connected (7 columns and 13 rows) connected in series. The active area of the cell was 7.2 cm^2. Total area of the solar cell module is 655.2 cm^2.
11.	PET/Indium tin oxide/Zinc oxide / PEDOT:PSS/ P3HT:PCBM/ Aluminium (Normal) [113]	Viscosity, screen resolution (200 μm)	P3HT:PCBM	110 °C for 30 min		1.8216 × 10^{-7} %	ZnO coating increases the surface roughness
12.	Glass/ITO/PEDOT:PSS/ P3HT:PCBM/Al [114]	Screen mesh (count 400), screen material (stainless steel), squeegee material, squeegee shape, squeegee angle (63○), squeegee speed (16.8 m/min) and squeegee pressure	P3HT: PCBM	150 °C for 30 min	0.09 cm^2	4.23 %	
13.	PET/PEDOT: PSS/Zinc oxide /P3HT: PCBM/PEDOT: PSS/ PET [115]	Rotary screen printing machine with speed >10 mm^{-1}	PEDOT: PSS	For drying, Drier of length 2 m is used.	≤ 10 mm^{-1}	1.6 % (carbon) 1.9 % (silver)	Three modules with sixteen serially connected cell are switched in parallel.
14.	PET/ITO/ZnO/Polymer/ PC$_{60}$BM PEDOT: PSS/silver grid [116]	NA	Silver grid back electrode	140 °C	4 cm^2	0.07 % (P1) 0.55 % (P2) 0.15 % (P30	
15.	Glass/Indium tin oxide /Zinc oxide/ P3HT: PCBM/ PEDOT: PSS/ silver [117]		Silver	140 °C for 2 min	0.5 cm^2	0.7 %	
16.	PET/Indium tin oxide /Zinc oxide / P3CT-ZnO/ PCBM/PEDOT/ silver [118]	PEDOT: PSS (165 mesh screen) printing speed 525 mm S^{-1}, silver back electrode (120 mesh screen),	Silver back electrode and PEDOT: PSS	Hot air oven for a duration of 15 min at a temperature of 130 °C.	1 stripe active area 15 cm^2	0.12 (1 stripe) 0.11 (2 stripe) 0.12 (3 stripe) 0.05 (8 stripe)	PEDOT sheet resistance 200-300 Ω/□. Silver 0.03-0.1 Ω/□.
17.	Insulated steel/Aluminium /Zinc oxide /P3HT:PC$_{61}$BM/PEDOT:PSS/ silver grids [119]	460 mesh screen	PEDOT:PSS	50 °C for 5 min 130 °C for 3 min	0.09 cm^2	0.7 %	PEDOT: PSS is mixed with IPA and Fluoro surfactant to print on hydrophobic active layer

Table 8
A list of OSCs fabricated with inkjet printing process with the details about the printer parameters and process parameters.

S.No	Device structure & geometry	Inkjet printer & Printing parameters	Inkjet printed layers	Annealing temperature in ◦C and Thickness in nm	Active area	PCE %	Remark
1.	Glass/ITO/P3HT: PCBM /Ca /Al Normal [36]	*Single piezo dispenser* 50 μm orifice Printing speed, overlap ratio	ITO, 750 nm thick, sheet resistance 202.7 Ω/□ and transmittance 84.14 %. Resistivity 1.52×10^{-2}	450 °C for 4 min.750 nm	4.66 mm^2	0.25 % (before annealing) 2.13 % (after annealing)	Rms roughness 11.1 nm
2.	Glass/Indium tin oxide / PEDOT: PSS / P3HT:PCBM / Lithium fluoride/Aluminium (Normal) [50]	*UJ 2100 Unijet*	PEDOT: PSS Additives 6 % glycerol and 0.2 % EGBE.	140 °C for 20 min	3 mm^2	2.09 % without additives and 3.6 % with additives.	Surface roughness of PEDOT:PSS with out additives 6.67 nm, with additives 1.36 nm.Conductivity of PEDOT:PSS 7.82×10^{-1} to 1.52×10^{2} S/cm.
3.	Glass/Indium tin oxide /Zinc oxide /P3HT: PCBM / Molybdenum triox-ide/silver.Glass/Mo/Al/Mo/ ZnO/P3HT:PCBM/Molybdenum trioxide/silver (Inverted) [61]	*LP50 pixdro* Print head (KM 512 L,3.5 cm width and 360 DPI)	ZnO, PEDOT: PSS and P3HT:PCBM	PEDOT: PSS 130 °C for a duration of 6 min, ZnO 130 °C for a duration of 1 min and photoactive layer 80 °C for 30 seconds 240 nm (active layer) 100 nm PEDOT: PSS	92 cm^2.	1.98 MPP mW /cm^2 1.78 mW /cm^2	Solvents for photoactive layer-o-xylene, indan and tetralin (1:1:1)
4.	Glass/Indium tin oxide /PEDOT: PSS/P3HT: PCBM/Lithium fluoride /Aluminium (Normal) [69]	*Microfab* Print on fly mode	PEDOT:PSS P3HT:C$_{60}$	PEDOT:PSS 200 °C for 5 min 100 nm (P3HT:C$_{60}$)	0.45 cm^2	0.0003	
5.	Glass / Indium tin oxide / PEDOT: PSS/ P3HT: PCBM/Aluminium (Normal) [71]	*Dimatix* Substrate temperature 40 °C. oDCM, mesitylene and tetralene	P3HT:PCBM	140 °C for 10 min 200 nm	20 mm^2 to 1 cm^2	2.9	ODCB and tetralene
6.	Glass/Indium tin oxide / PEDOT: PSS/ P3HT: PCBM/ Calcium/ silver (Normal) [72]	*Dimatix* Substrate temperature, inkjet latency time, inkjet drying time. Drop spacing 35 μm for RR 96 %. 6 to 9 m/s is the drop velocity and 10 pl is the drop volume.	P3HT RR 98.5 % P3HT RR 93 % Solvent ODCB and mesitylene	140 °C for 10 min 200 nm	20 mm^2 to 1 cm^2	1.29 (RR93% tetralene) 3.47 % (RR 96 % oDCB /mesitylene)	
7.	Glass/Indium tin oxide /PEDOT: PSS/PFDTBTP: PC6$_1$BM/Lithium fluoride/ Aluminium (Normal) [75]	*Dimatix DMP 2800*	PFDTBTP: PC$_{61}$BM, PEDOT:PSS grids over PEDOT:PSS layer.	80 °C for 5 min 120 nm	0.6 cm2	3% with chlorinated 2% with non chlorinated (anisole /tetralin)	Rms spin coated film 0.5 nm, inkjet printed 1.1 nm with chlorinated and 1.4 nm with non-chlorinated solvents.
8.	Glass/Indium tin oxide/ PEDOT: PSS/ PFDTBTP: PC$_{61}$BM/ Lithium fluoride/Aluminium (Normal) [76]	*LP 50 (pixdro)*	PFDTBTP: PC$_{61}$BM solvents anisole, p-xylene, mesitylene and tetralin.	80 °C for 5 min 81 nm	59.5 mm^2	Chlorinated 3.5 % Non chlorinated 2.7 %	
9.	Glass/PEDOT:PSS/ PCDTBT:PCBM/ ZnO /Ag(Normal) [78]	*Microfab* Normal	PEDOT:PSS, PCDTBT: PCBM (combination of chlorobenzene, mesitylene and chloroform),Zinc oxide and silver ink	120 °C for 15 min. 70 °C for 10 min 15 min at 80 °C. 120 nm	0.5 cm^2	CB:CF (1:1) 3% CB:MT (1:1) = 4 % CB:MT: CF (5:4:1)=4.85 % ZnO quantum dot 2.05 % and zinc oxide nano rod 0.76%.	surface roughness of inkjet printed film 4.65 nm, spin coated film 1.31 nm.

10.	Glass/Ag lines/PEDOT:PSS/ P3HT:PCBM/LiF/ Aluminium (Normal) [104]	*Dimatix DMP 2800* 10 PL catridge, drop spacing 40 μm, silver lines (height 250 nm and width 100 μm. Firing voltage 29 V, 13 m/s is the ejection speed.	Silver grids	150 °C for 20 min.130 nm	25 mm^2	2.15 % (ITO), embedded (2.54 %) silver grid, not embedded 1.70 %.	Reverse nano printing
11.	Glass/Indium tin oxide/PEDOT: PSS/P3HT:PCBM/ Zinc oxide /silver (Normal) [107]	*UJ2100* The contact angle of silver ink over P3HT:PCBM is 47○. It is reduced to 15° after coating with Zinc oxide.	Silver back electrode	120 °C		0.2 % (annealing of ZnO at 150 °C)	P3HT: PCBM is hydrophobic in nature. Hydrophilic ZnO nanorods were coated over the P3HT:PCBM layer and then silver back electrode is inkjet printed.
12.	PET (Roll) /Ag grid / PEDOT: PSS / Zinc oxide / P3HT: PCBM/ PEDOT: PSS/Ag (Inverted) [110]	*DOD printer with Kyocera print heads* Speed 2 m/min^{-1} and sheet resistance 38 Ω/□.	Back electrode silver ink	140 °C for 2 min 0.5 μm		0.83 %	Corona treatment to achieve wetting of the water-based ink.
13.	Glass/Indium tin oxide /PEDOT: PSS / P3HT: PCBM /Aluminium (Normal) [120]	*Dimatix 2831* Substrate temperature 40 °C. Solvent 1:1 volume of tetraline and chlorobenzene	P3HT:PCBM solvent Tetraline and chlorobenzene32%	160 nm	0.03 cm^2	1.4 %	Viscosity 6.1 mPa S, surface tension 35.2 mN/m. The coffee ring effect was observed at 1 % concentration 104.
14.	Glass/PEDOT: PSS/P3HT: PCBM/Calcium /Aluminium (Normal) [121]	*Aurel* Drop emission frequency, print head speed, substrate temperature Waveform 75 μs and 78 V. 70 μm print head, drop diameter 90 μm and 180 pl volume.	PEDOT:PSS with DMSO	150 °C for 1 hour	20 mm^2	1.5 %	
15.	Glass/silver grids/HC PEDOT:PSS/ P3HT:PCBM/ Calcium /Aluminium (Normal) [122]	*Dimatix DMP 2800* Drop spacing 25 μm, thickness - 250 nm, Width 200 μm and sheet resistance 5.8 Ω/□.	Silver grids	200○ for 10 min 250 nm	cm^2 4 cm^2	1.93 % 0.17 %	Pitch size 3,5 and 10 mm
16.	Glass/Indium tin oxide /Zinc oxide/ P3HT:PCBM / PEDOT:PSS/silver (Inverted) [123]	*DOD printer*	Silver grids Width 46 μm and height 200 nm	100 °C for 20 min 46 μm width and 200 nm height	9 mm^2	1.96 %	PEDOT: PSS and active layer doctor bladed.
17.	Glass/cu grids/ PEDOT:PSS/ Si-PCPDTBT :PCBM/ca/Al. (Normal) [124]	*Dimatix* Drop spacing 25 μm	Copper grids	60 °C for one hour Height 450 nm width 80-85 μm.	9 mm^2	3.35 % Embedded 2.56 %	Laser sintering

Table 8 (*Continued*)

S.No	Device structure & geometry	Inkjet printer & Printing parameters	Inkjet printed layers	Annealing temperature in ∘C and Thickness in nm	Active area	PCE %	Remark
18.	Glass/Indium tin oxide/ PEDOT:PSS / P3HT:PCBM/ Lithium fluoride/ Aluminium. (Normal) [125]	*Unijet UJ 2100* Print head and substrate temperature 26 °C	PEDOT:PSS additives Ethylene glycol butyl ether (0.0140) glycerol (0.431) P3HT:PCBM in chlorobenzene additives: ODT, ODCB and cl-napth	140 °C for 20 min.150 nm	9 mm^2	3.71 %	Surface roughness without additives 64 nm with additives 17 to 21 nm. Xrd peak intensity 2θ = 5.3
19.	Glass/silver grids/ PEDOT:PSS/LiF /Al(Normal) [126]	*Dimatix* Drop spacing 30 μm	Silver grids, PEDOT:PSS	130 °C for 30 min. 400 nm (silver grids) 100 nm(PEDOT:PSS)	2 × 2 cm^2	1.54 %	
20.	Glass/Indium zinc tin oxide / PEDOT:PSS/ P3HT:PCBM/ Calcium/ Aluminium (Normal) [127]	*Omni 200 (unijet)* With 19 μm print head from Samsung Printing speed, overlap ratio, Line to line pitch -50 μm Sheet resistance 20.6 Ω/□. Optical transmittance – 81.29%	Indium zinc tin oxide	400 °C -700 °C in nitrogen / oxygen atmosphere 1.5 μm	4.6 mm^2	0.81 %	
21.	Glass/Indium tin oxide/ PEDOT:PSS/ P3HT:PCBM /Calcium /Aluminium (Normal) [128]	*Single piezo -dispenser* (50 μm orifice diameter) Average transmittance 81.9 %, sheet resistance 198.8 Ω/□. 50 μm print head.	ITO	450 °C for 4 min. 800 nm	0.0625 0.09 0.29 0.49	1.8 1.8 1.6 1.3	Rms roughness 12 nm.
22.	Glass/ITO/ZnO/P3HT: ICBA nanoparticles/ PEDOT:PSS/Ag. (Inverted) [129]	*Dimatix DMP 2831* Platen temperature 40 °C	P3HT:ICBA in 2-butoxy ethanol ZnO printed with 50 μm print head. Tungsten oxide PEDOT:PSS	150 °C for a duration of 10 min 85 °C for a duration of 10 min. 120 °C for a duration of 10 min 25 μm (WO$_3$) 25 μm (PEDOT: PSS)	0.105 cm^2 1.1 cm^2	3.9 % 3.4 %	8 sub layers were inkjet printed (drop spacing 65 μm) and 8 sub layer were inkjet printed (drop spacing 35 μm.)
23.	Glass/silver /HC PEDOT/Zinc oxide/ P3HT:PCBM /PEDOT: PSS/ Silver (Inverted) [130]	*Dimatix DMP 2831* Drop pitch, line pitch, surface temperature.	Silver fingers and bus bars (Dimatix DMP 2831). HC PEDOT, Zinc oxide nanoparticles, the photoactive layer and PEDOT (LP50 printing platform with halogenated solvents only).	130 °C for 10 min. Photoactive layer (240 nm) 200 nm (PEDOT)	6.24 cm^2	4.1 % (all inkjet printed)	Photoactive layer non chlorinated solvents 0-Oxylene, indane and tetralin (1:1:1) with P3HT and PCBM in 1.3 wt % concentration
24.	Glass/silver nanowires/Zinc oxide / PV2000:PC$_{71}$BM/ PEDOT:PSS/ silver (Inverted) [131]	*Pixdro LP50* Inkjet printing four times, 0.5 Ω/□ is the sheet resistance.	Silver nanowire, ZnO, PV2000:PC71BM (mixture of xylene and tertraline 1:1), PEDOT: PSS.	120 °C for 5 min (AgNW) 140 °C for 5 min. AgNW 110 nm Active layer (550 nm) PEDOT: PSS (320 nm) AgNW (110 nm)	1 cm^2	4.3 %	

screen printed films is about 5–100 μm. Because of the higher thickness, efficiency of rotary screen printing is less than flat bed screen printing. In inkjet printing, a thin layer of ink of very low viscosity is printed over the underlying layers. Defects in the underlying layers affect the quality of the printed film [110]. In another set of experiments, comparison is made between inkjet printed and evaporated back electrodes, where the efficiency achieved in both the processes is almost the same. The fill factor of inkjet printed grids is higher than the evaporated electrodes as a result of comparatively higher thickness in inkjet printing.

OSCs are screen printed with a 120 mesh screen on the screen printed PEDOT:PSS layer and after printing annealing is performed at a temperature of 130 °C for a duration of 3 min, the sheet resistance of the electrodes is in the range 0.03 to 0.1 $\Omega/\square$. The efficiency of the solar cell is 0.0013% [54].

OSCs are fabricated with silver as the top electrode (screen printed). The sheet resistance of the screen-printed silver for a thickness of 15 μm is 0.06 $\Omega/\square$. The screen printed silver has a sheet resistance of 0.06 $\Omega/\square$ for a thickness of 15 μm. The surface morphology and surface roughness of the screen-printed films are examined, and the characteristics of the solar cell thus fabricated are compared with the ones with vacuum processed electrodes. FESEM confirms the uniformity of the void free printed films, which resulted in enhanced charge induction and hence reduced sheet resistance of the printed layer. Generally the screen printed layers exhibit a high roughness value because of the various printing parameters involved such as mesh count, squeeze pressure, speed and angle. The average surface roughness of the screen-printed back electrode silver layer, R_{rms} = 178 nm, which has a negative effect on charge conduction. The solar cell device fabricated with the geometry ITO /Zinc oxide /P3HT: PCBM/PEDOT: PSS/silver exhibited a Power conversion efficiency of 2.58% [111]. The FESEM and AFM of the screen- printed back electrode is shown in Fig. 12.

Comparison between the inkjet printing and the screen-printing process for printing conductive inks in terms of printing parameters, annealing, sheet resistance, optical transmittance and the efficiency is shown in Table 6. The list of screen printed and inkjet printed OSCs fabricated by various research groups throughout the world in both the normal and inverted geometry are shown in Table 7 [35,46,55,63–68,81,84,85,95–106], respectively (Fig. 12).

4. Conclusions

Both screen printing and inkjet printing are being used by researchers to produce OSCs. Among the two, inkjet printing is preferred most because of less material wastage, no screen or stencil preparation, ability to print small volumes of ink, no need to clean the image carrier after printing, high resolution and suitability for mass production. But screen printing itself has its own advantages such as uniform film, higher thickness, low cost of equipment, quick turn around and less smearing. Screen printing is mainly used for printing busbars and fingers in silicon solar cells along with OSCs. The viscosity of the screen-printing ink should be high to prevent flow of inks through the mesh without any external pressure. Some of the materials used in OSCs such as photoactive layer is of very low viscosity. Thermocleavage solvents with high viscosity are used to print such type of materials. Another major concern in screen printing is the higher thickness of the printed layers. Nowadays, it is possible to print screen printed layers of thickness less than 20 nm by careful selection of the screen material, mesh count and solution concentration. The inkjet printing also has its own restrictions such as low viscosity inks, clogging of nozzles and shorter distance between the printhead and the substrate. To overcome this constraints, new methods of inkjet printing technologies such

as aerosol inkjet printing and electrohydrodynamic inkjet printing are being developed. Nevertheless, a combination of screen printing and inkjet printing is always a better option for the mass production of OSC. The inkjet printing could be utilized for printing thinner layers such as the electron and the hole transport layers, and the screen printing could be utilized for printing thicker layers such as the photoactive layer and the back electrodes.

The potential of combination of these two technologies for printing OSC, is currently not utilized fully and we anticipate that more combination works are likely to emerge in the near future. Both the screen and inkjet printing process should be customized to handle a range of inks with different rheological properties. The integration of the two processes along with other analytical systems such as dryers is critical in determining the quality of the end product. The combination of these technologies can be applied not only to the printing of OSCs, it can also be elaborated to other functional devices such as organic light emitting diodes. The combination of inkjet printing and screen-printing processes will help in producing low cost OSCs with better device performance in the near future.

CRediT authorship contribution statement

S. Ganesan: Data curation, Software, Validation, Writing - original draft. **S. Mehta:** Conceptualization, Methodology, Visualization, Investigation. **D. Gupta:** Supervision, Writing - review & editing.

Acknowledgements

References

[1] B. Derby, Inkjet printing of functional and structural materials: fluid property requirements, feature stability, and resolution, Annu. Rev. Mater. Res. 40 (2010) 395–414.

[2] J.Y. Park, Ge. Gao, J. Jang, D.W. Cho, 3D printed structures for delivery of biomolecules and cells: tissue repair and regeneration, J. Mater. Chem. B Mater. Biol. Med. 4 (2016) 7521–7539.

[3] G. Kaur, R. Adhikari, P. Cass, M. Bown, P. Gunathilake, Electrically conductive polymers and composites for biomedical applications, RSC Adv. 5 (47) (2015) 37553–37567.

[4] R. Sondergaard, M. Hosel, D. Angmo, T.T.L. Olsen, F.C. Krebs, Roll -to-roll fabrication of polymer solar cells, Mater. Today 15 (2012) 36–49.

[5] N. Marinova, S. Valero, J.L. Delgado, Organic and perovskite solar cells: working principles, materials and interfaces, J. Colloid Interf. Sci. 488 (2017) 373–389.

[6] R. Das, K.G. Zadeh, G. Chanson, X. He, Flexible, Printed and Organic Electronics Forecasts, Player & Opportunities, 2017–2027, Idtech ex Cambridge, UK, 2016.

[7] K. Suganuma, Introduction to printed electronics, Springer Briefs in Electrical and Computer engineering, 2014, 25, ISBN 2191–8120.

[8] J.E. Fromm, Numerical calculation of the fluid dynamics of drop on demand jets, IBM J. Res. Dev. 28 (1984) 322–323.

[9] N. Reis, C. Ainsley, B. Derby, Inkjet delivery of particle suspensions by piezoelectric droplet ejectors, J. Appl. Phys. 9 (2005) 094903–094906.

[10] D. Jang, D. Kim, J. Moon, Influence of fluid physical properties on inkjet printability, Langmuir 25 (2009) 2629–2635.

[11] A.A. Goghari, S. Chandra, Producing droplets smaller than the nozzle diameter by using a pneumatic drop on demand droplet generator, Exp. Fluids 44 (2008) 105–114.

[12] R.D. Deegan, O. Bakajn, T.F. Dupont, G. Huber, S.R. Nagel, T.A. Written, Capillary flow as the cause of ring stains from dried liquid drops, Nature 389 (1997) 827–829.

[13] H. Hu, R.G. Larson, The Marangoni effect reverses coffee ring depositions, J. Phys. Chem. B 110 (2006) 7090–7094.

[14] P.Y. Yunker, Tim still, Suppression of the coffee ring effect by shape-dependent capillary interactions, Nature 476 (2011) 308–311.

[15] D. Soltman, V. Subramanian, Inkjet printed line morphologies and temperature control of the coffee ring effect, Langmuir 24 (2008) 2224–2231.

[16] L. Cui, J. Zhang, X. Zhang, L. Huang, Z. Wang, Y. Li, H. GAO, S. Zhu, T. Wang, B. Yang, Suppression of the coffee ring effect of hydro soluble polymer additives, ACS Appl. Mater. Interfaces 4 (2012) 2775–2780.

[17] J. Park, J. Moon, Control of colloidal particle deposit patterns with in picoliter droplets ejected by inkjet printing, Langmuir 22 (2006) 3506–3513.

[18] Y. Oh, H.G. Yoon, S.N. Lee, H. Ki Kim, J. Kim, Inkjet printing of TiO2 cosolvent ink: from uniform ink droplet to TiO2 photo electrode for dye sensitized solar cells, J. Electrochem. Soc. 159 (2012) B34–B38.

[19] D.Kim S. Jeong, B.K. Park, J. Moon, Direct writing of silver conductive patterns: improvement of film morphology and conductance by controlling solvent compositions, Appl. Phys. Lett. 89 (2006) 264101–264103.

[20] D.E. Riemer, The theoretical fundamentals of the screen printing process, Microelectron. Int. 6 (1989) 8–17.

[21] S. Abbott, How to be a great screen printer, the theory and practice, Macdermid Autotype (2008), ISBN: 978-0-9551220-1-9.

[22] F.C. Krebs, Fabrication and processing of polymer solar cells-A review of printing and coating techniques, Sol. Energy Mater. Sol. Cells 93 (2009) 394–412.

[23] S. Mehta, S. Murugesan, B. Prakash, A. Deepak, Novel living ink based on Saccharomyces cerevisae for the screen printing process and its applicability in producing braille text dots, Mater Today Commun 15 (2018) 325–332.

[24] K. Futera, M. Jakubowska, Printed electronics on flexible and glass substrates, Photonics Lett. Pol. 2 (2010) 85–87.

[25] K. Schulze, B. Maennig, K. Leo, Organic solar cells on indium tin oxide and aluminium doped zinc oxide anodes, Appl. Phys. Lett. 91 (2007) 073521–073523.

[26] K.H. Choi, J.A. Jeong, H.K. Kim, Dependence of electrical, optical and structural properties on the thickness of IZTO thin films grown by linear facing target sputtering for organic solar cells, Sol. Energy Mat. Sol. C 94 (2010) 1822–1830.

[27] W.A. Mac Donald, M.K. Looney, D.M. Kerron, R. Eveson, R. Adam, K. Hashimoto, K. Rakos, Latest advances in substrates for flexible electronics, J. Soc. Inf. Disp. 15 (2007) 1075–1083.

[28] A. Huebler, B. Trnovec, T. Zillger, M. Ali, N. Wetzold, M. Mingebach, A. wagenfahl, C. Deibel, V. Dyakonov, Printed paper photovoltaic cells, Adv. Energy Mater. 1 (2011) 1018–1022.

[29] L. Leonat, M.S. White, E.D. Glowacki, M.C. Scharber, T. Zilliger, J. Ruhling, A. Huebler, N.S. Sariciftci, 4% efficient polymer solar cells in paper substrates, J. Phy. Chem C 118 (2014) 16813–16817.

[30] Y. Galagan, D.J.D. Moet, D.C. Hermes, P.W.M. Blom, R. Andriessen, Large area ITO free organic solar cells on steel substrate, Org. Electron. 13 (2012) 3310–3314.

[31] L. Wong, C.M. Ho, Surface molecular property modifications for (polydimethylsiloxane) PDMS based microfluidic devices, Microfluid Nanofluid 7 (2009) 291–306.

[32] V. Zardetto, T.M. Brown, A. Reale, A.D. Carlo, Substrates for flexible electronics: a practical investigation on the electrical, film flexibility, optical, temperature and solvent resistance properties, J. Polym. Sci.: Polym. Phys. Ed. 49 (2011) 638–648.

[33] Z.Y. Hui, M.Z. Xia, L.H. Li, D.X. Long, Review of flexible and transparent thin film transistors based on zinc oxide and related materials, Chin. Phys. B 26 (2017) 047307.

[34] Martin Weis, Transparent electrodes for flexible organic light emitting diodes and displays, Disp. Imaging 2 (2015) 49–68.

[35] B.W.N.H. Hemasiri, J.K. Kim, J.M. Lee, Fabrication of highly conductive graphene ITO transparent bi film through CVD and organic additives free sol-gel techniques, Sci. Rep. 7 (17868) (2017) 1–12.

[36] M.S. Hwang, B.Y. Jeong, J. Moon, S.K. Chun, J. kim, Inkjet printing of indium tin oxide (ITO films) for transparent conducting electrodes, Mater. Sci. Eng. B 176 (2011) 1128–1131.

[37] P. Reddy Matli, R.A. Shakoor, A. Mohamed, A. Mohamed, M. Gupta, Microwave rapid sintering of Al-metal matrix composites: a review on the effect of reinforcement microstructure and mechanical properties, Met. 6 (2016) 143 (19 pages).

[38] D. Chen, C. Jiang, H. Sun, B. Feng, X. Lu, J. Weng, J. Wang, Sintering study of ITO using a ZnO doped and microwave hybrid sintering approach, J.A. Ceram. Soc 2 (2014) 57–63.

[39] J.A. Jeong, J. Lee, H. Kim, H.K. Kim, S.I. Na, Inkjet printed transparent electrode using nano-size indium tin oxide particles for organic photovoltaics, Sol. Energy Mater. Sol. Cells 94 (2010) 1840–1844.

[40] J.A. Jeong, H.K. Kim, J. kim, Invisible Ag grid embedded with ITO nanoparticle layer as a transparent hybrid electrode, Sol. Energy Mater. Sol. Cells 125 (2014) 113–119.

[41] B. Bessais, N. Mliki, R. Bennaceur, Technological structural and morphological aspects of screen printed ITO used in ITO/si type structure, Semicond. Sci.Technol 8 (1993) 116–121.

[42] B. Bessais, H. Ezzaouia, R. Bennaceur, Electrical behaviour and optical properties of screen printed ITO thin films, Semicond. Sci. Technol. 8 (1993) 1671–1678.

[43] R. Po, C. Carbonera, A. Bernardi, Nadia Camaioni, The role of buffer layers in polymer solar cells, Energy Environ. Sci. 4 (2011) 285–310.

[44] F. Wang, Z. Tan, Y. Li, Solution processable metal oxides/chelates as electrode buffer layers for efficient and stable polymer solar cells, Energy Environ. Sci. 8 (2015) 1059–1091.

[45] S. Lattente, Electron and hole transport layers: their use in inverted bulk heterojunction polymer solar cells, Electron 3 (2014) 132–164.

[46] E.D. Gomez, Y.L. Loo, Engineering the organic semiconductor electrode interface in polymer solar cells, J.Mater.Chem 20 (2010) 6604–6611.

[47] S.D. Hoath, W.K. Hsiao, G.D. Martin, S. Jung, S.A. Butler, N.F. Morrison, O.G. Harlen, L.S. Yang, C.D. Bain, I.M. Hutchings, Oscillations of aqueous PEDOT:PSS droplets and the properties of complex fluids in drop-on-demand inkjet printing, J. Non-Newton Fluid 223 (2015) 28–36.

[48] A. Singh, S. Mandal, V. Singh, A. Garg, M. Katiyar, Inkjet printed PEDOT:PSS for organic devices, 6th international workshop on physics of semiconductor devices, Proc. SPIE 8549 (2012) 854936.

[49] A. Singh, M. Katiyar, Ashish Karg, understanding the formation of PEDOT:PSS films by inkjet printing for organic solar cell applications, RSc Adv.5 (2015) 78677–78685.

[50] S.H. Eom, S. Sundaram, P. Uthirakumar, S.C. Yoon, J. Lim, C. Lee, H.K. Lim, J. Lee, S.H. Lee, Polymer solar cells based on inkjet printed PEDOT:PSS layer, Org. Electron. 10 (2009) 536–542.

[51] K.X. Steirer, J.J. Berry, M.O. Reese, M.F.A.M. Van Hest, A. Miedaner, M.W. Liberatore, R.T. Collins, D.S. Ginley, Ultrasonically sprayed and inkjet printed thin film electrodes for organic solar cells, Thin Solid Films 517 (2009) 2781–2786.

[52] S.S. Yoon, D.Y. Khang, Roles of Nonionic surfactant additives in PEDOT:PSS thin films, J. Phys Chem C 120 (2016) 29525–29532.

[53] X. Hu, G. Chen, X. Wang, H. Wang, Tuning thermoelectric performance by nanostructure evolution of a conducting polymer, J. Mater. Chem. A 3 (2015) 20896–20902.

[54] F.C. Krebs, M. Jorgensen, K. Niorrmann, O. Hagermann, J. Alstrup, T.D. Nielsen, J. Fyenbo, K. Larsen, J. Kristensen, A complete process for production of flexible large area polymer solar cells entirely using screen printing-first public demonstration, Sol. Energy Mater. Sol. Cells 93 (2009) 422–441.

[55] C. Yi, X. Gong, Towards high performance inverted polymer solar cells, Current Opin. Chem. Eng 53 (2012) 5437–5448.

[56] Z. Liang, Q. Zhang, L. Ziang, G. CaO, Zinc oxide cathode buffer layers for inverted polymer solar cells, Energ Environ. Sci. 8 (2015) 3442–3476.

[57] B. Qui, Z.G. Zuang, Jizheng Wang, Uncovering the role of cathode buffer layer in organic solar cells, Sci. Rep. 5 (7803) (2015) 1–78038.

[58] N.A. Jayah, H. Yahaya, M.R. Mahmood, T. Terasako, K. Yasui, A.M. Hashim, High electron mobility and low carrier concentration of hydrothermally grown ZnO thin films in seeded α plane sapphire at low temperature, Nanoscale Res. Lett. 10 (2015) 7.

[59] I. Ullah, S.K. Shah, S. Wali, K. Hayat, S.A. Khattak, A. Khan, Enhanced efficiency of organic solar cells using ZnO as an electron transport layer, Mater. Res. Express 4 (2017) 125505.

[60] A. Singh, S. Gupta, A. Garg, Inverted polymer bulk heterojunction solar cells with inkjet printed electron transport and active layers, Org. Electron. 35 (2016) 118–127.

[61] T.M. Eggenhuisen, Y. Galagan, E.W.C. Coenen, W.P. Voorthuijzen, M.W.L. Slaats, S.A. Kommeren, S. Shanmuganam, M.J.J. Coenen, R. Andriessen, W.A. Groen, Digital fabrication of organic solar cells by inkjet printing using non-halogenated solvents, Sol. Energy Mater. Sol. Cells 134 (2015) 364–372.

[62] J.G. Sanchez, V.S. Balderarrama, S.I. Garduno, E. Osorio, A. Viterisi, M. Estrada, J. Ferre-Borrull, J. Pallares, L.F. Marsal, Impact of inkjet printed ZnO electron transport layer on the characterization of polymer solar cells, RSc. Adv. 8 (2018) 13094–13102.

[63] R.A. Zargar, S. Chackrabarti, S. Joseph, M.S. Khan, R. Husain, A.K. Hafiz, Synthesis and characterization of screen printed ZnO films for solar cell applications, Optik 126 (2015) 4171–4174.

[64] B. Ismail, M. Abaab, B. Rezig, Structural and electrical properties of ZnOfilms prepared by screen printing technique, Thin Solid Films 383 (2001) 92–94.

[65] H.M. Zhou, D.Q. Yi, Z.M. Yu, L.R. Xiao, J. Li, Preparation of aluminium doped zinc oxide films and study of their microstructure,electrical and optical properties, Thin Solid Films 515 (2007) 6909–6914.

[66] D. Lidzay, D.D.C. Bradley, M.S. Skolnick, T. Virgili, S. Walker, D.M. whittaker, Strong exciton photocouplingin an organic semiconductor microcavity, Nature 395 (1998) 53–55.

[67] M. Knupper, Excitons binding energies in organic semiconductors, Appl. Phys.A. 77 (2003) 623–626.

[68] A.K. Kleinschmidt, S.E. Root, D.J. Lipomi, poly(3-hexylthiopene)P3HT:fruit fly or outlier in organic solar cell, J. Mater. Chem. A 5 (2017) 11396–11400.

[69] V.G. Shah, D.B. Wallace, Low cost solar cell fabrication by drop on demand inkjet printing, Proc.IMAPS 37th annual international symposium in microelectronics, Long Beach (2004) 14–18.

[70] J. Kim, C. Park, I. Song, M. Lee, H. Kim, H.C. Choi, Unique crystallization of fullerenes:fullerene flowers, Sci. Rep. 32205 (2016) 1–8.

[71] C.N. Hoth, S.A. Choulis, P. Schilinsky, S.A. Choulis, C.J. Brabec, High photovoltaic performance of inkjet printed polymer fullerene blends, Adv. Mater 19 (2007) 3973–3978.

[72] C.N. Hoth, P. Schilinsky, S.A. Choulis, C.J. Brabec, Printing highly efficient organic solar cells, Nanolett. 8 (2008) 2806–2813.

[73] P. Schilinsky, U. Asawapirom, U. Scherf, M. Biele, C.J. Brabec, Influence of the molecular weight of (poly(3-hexylthiophene) on the performance of bulk heterojunction solar cells, Chem. Mater. 17 (8) (2005) 2175–2180.

[74] Ch. Liu, K. Wing, Xi. Hu, Y. Yang, Ch.-H.O. Hsu, W. Zhang, S. Xiao, X. Gong, Y. CaO, Molecular weight effect on the efficiency of polymer solar cells, ACS Appl. Mater. Interfaces 5 (2013) 12163–12167.

[75] A. Lange, M. Wegener, B. Fischer, S. Janietz, A. Wedel, Solar cells with inkjet printed polymer layers, Energy Procedia 31 (2012) 150–158.

[76] A. Lange, W. Schindler, M. Wegener, K. Fostiropoulos, S. Janietz, Inkjet printed solar cell active layers prepared from chlorine free solvent systems, Energy Mater. Sol. Cells 109 (2013) 104–110.

[77] T.M. Eggenhuisen, Y. Galagan, E.W.C. Coenen, W.P. Voorthuijzen, M.W.L. Slaats, S.A. Kommeren, S. Shanmuganam, M.J.J. Coenen, R. Andriessen, W.A. Groen, Digital fabrication of organic solar cells by inkjet printing using non-halogenated solvents, Sol. Energy Mater. Sol. Cells 134 (2015) 364–372.

[78] S. Jung, A. Sou, K. Banger, D.H. Ko, P.C.Y. Chow, C.R. Mc Neill, H. Sirringhaus, All-inkjet printed, All-air-processed solar cells, Adv. Energy.Mater. 4 (2014) 1400432.

[79] S.E. Shaheen, R. Radspinner, N. Peyghambarian, G.E. Jabbour, Fabrication of bulk heterojunction plastic solar cells by screen printing, Appl. Phys. Lett. 79 (2001) 2996–2998.

[80] J. Sakai, E. Fujinaka, T. Nishomori, N. Ito, J. Adachi, S. Nagano, K. Murakami, High Efficiency Organic Solar Cells by Screen Printing Method, Conference Record of the Thirty First IEEE, Photovoltaic Specialists Conference, 2005, 125–128.

[81] T. Aeronauts, P. Vanlaeke, J. Poortmans, P.L. Heremans, Polymer Solar Cells; Screen Printing as a Novel Deposition Technique, Proceedings of SPIE Vol 5464, Organic Optoelectronics and Photonics, Photonics Europe Strasbourg, France, 2004, 252–260.

[82] K. Koynov, A. Bahtiar, T. Ahn, R.M. Cordeiro, H.H. horhold, C. Bubeck, Molecular weight dependence of chain orientation and optical constants of thin films of the conjugated polymer MEH-PPV, Macromolecules 39 (2006) 8692–8698.

[83] F.C. Krebs, J. Alstrup, H. Spanggard, K. Larsen, E. Kold, Production of large area polymer solar cells by industrial silk screen printing, life time, considerations and lamination with polyethylene terephalate, Sol. Energy Mater. Sol. Cells C 83 (2004) 293–300.

[84] M. Jorgenson, O. Hagemann, J. Alstrup, F.C. Krebs, Thermoclevable solvents for printing conjugated polymers, Application in polymer solar cells, Sol. Energy Mater. Sol. Cells 93 (2009) 413–421.

[85] A. Khalate, X. Bombois, G. Scorletti, R. Babuska, S. Koekebakker, W.D. Zeeuw, A waveform design method for a piezo inkjet printhead based on Robust feed forward control, J. Microelectromech. Syst. 21 (2012) 1365–1374.

[86] H.Y. Gan, X. Chan, T. Eriksson, B.K. Lok, Y.C. Lam, Reduction of droplet volume by controlling actuating waveforms in inkjet printing for micropattern formation, J. Micromech. Microeng. 19 (055010) (2009) 1–8.

[87] C.F. Liu, Y. Lin, W.Y. Lai, W. Huang, Improved performance of inkjet printed Ag source drain electrodes for organic thin film transistors by overcoming the coffee-ring effects, AIP Adv. 7 (115008) (2017) 1–1150087.

[88] M. Ikegawa, H. Azuma, Droplet behaviours on substrates in thin film formation using inkjet printing, JSME INT Series B 47 (2004) 490–496.

[89] Y. HaO, J. GaO, Z. Xu, N. Zhang, J. LuO, X. Liu, Preparation of silver nanoparticles with hyper branched polymers as a stabilizer for inkjet printing of flexible circuits, New. J. Chem. 43 (2019) 2797–2803.

[90] W. Yin, D.H. Lee, J. Choi, C. Park, S.M. Cho, Screen printing of silver nanoparticle suspension for metal inter connects, Korean J. Chem. Eng. 25 (6) (2008) 1358–1361.

[91] S.G.R. Avuthu, M. Gill, N. Ghalib, M. Sussman, G. Wable, J. Richstein, J. Circuit, An introduction to the process of printed electronics, in: proceedings of SMTA international, September 25–29, Rosemont, IL, 2016, 246–252.

[92] J. Pan, G.L. Tonkay, A. Quintero, Screen printing process design of experiments for fine line printing of thick film ceramic substrates, J. Electron Manuf. 9 (1999) 203–213.

[93] A. Willfahrt, J. Stephens, G. Hübner, Optimised stencil thickness and ink film deposition, Int. Circ. Educ. Inst. Graphic Arts 4 (2011) (2011) 6–17.

[94] R. Bennett, R. Lieske, C. Beech, Profiled Squeegee Blade:Rewrites the Rule for Angle of Attack, IPC APEX Expo Conference Proceedings, San Diego, California, 19–21, February, 2013, 2013, 1592–1605.

[95] H.-P. Kuo, C.-F. Yang, A.-N. Huang, C.-T. Wu, W.-C. Pan, Preparation of the working electrode of dye-sensitized solar cells: effects of screen-printing parameters, J. Taiwan Inst. Chem. Eng. 45 (2014) 2340–2345.

[96] W. Yin, D.H. Lee, J. Choi, C. Park, S.M. Cho, Screen printing of silver nanoparticle suspension for metal inter connects, Korean J. Chem. Eng. 25 (6) (2008) 1358–1361.

[97] X. Wang, L. Zhi, K. Mullen, Transparent conductive graphene electrodes for dyesensitized solar cells, Nanolett. 8 (2008) 323–327.

[98] N.F. Anglada, J.P. Puigdemont, J. Figueras, M.Z. Iqbal, S. Roth, Flexible, transparent electrodes using carbon nanotubes, Nanoscale Res. Lett. 7 (2012) 571.

[99] Z. Wu, Z. Chen, X. Du, J.M. Logan, J. Sippel, M. Nikolou, K. Kamaras, J.R. Reynolds, D.B. Tanner, A.F. hebard, A.C. Rinzler, Transparent Conductive Carbon Nanotube Films Sci. 305 (2004) 1273–1276.

[100] M. Vosqueritchian, D.J. Lipomi, Z.A. Bao, Highly conductive and transparent PEDOT:PSS films with a fluorosurfactant for stretchable and flexible transparent electrodes, Adv. Funct. Mater 22 (2012) 421–428.

[101] C. Bao, J. Yang, H. Gao, F. Li, Y. Yao, B. Yang, G. Fu, X. Zhou, T. Yu, Y. Qin, J. Liu, Z. Zou, In Situ fabrication of highly conductive metal nanowires networks with high transmittance from deep ultraviolet to Near-Infrared, ACS Nano 9 (2015) 2502–2509.

[102] T. Aeronauts, P. Vanlaeke, W. Geens, J. Poortmans, P. Heremans, S. Borghs, R. Mertens, R. Andriessen, L. Leenders, Printable anodes for flexible organic solar cell modules, Thin Solid Films 451–452 (2004) 22–25.

[103] Y. Galagan, J.E.J.M. Rubingh, R. Andriessen, C.C. Fan, P.W.M. Blom, S.C. Veenstra, J.M. Kroon, ITO free flexible organic solar cells with printed current collecting grids, Sol. Energy Mater. Sol. Cells 95 (2011) 1339–1343.

[104] I.B. Ceballos, N. Kehagias, C.M.S. Torres, M.C. Quiles, P.D. Lacharmoise, Embedded inkjet printed silver grids for ITO free organic solar cells with high fill factor, Sol. Energy Mater. Sol. Cells 127 (2014) 50–57.

[105] J.S. Yu, I. Kim, J.S. Kim, J. Jo, T.T. Larsen-Olsen, R.R. sondergaard, M. Hosel, D. Angmo, M. Jorgensen, F.C. krebs, Silver front electrode grids for ITO free all printed organic solar cells with embedded and raised topographies, prepared by thermal imprint, flexographic and inkjet roll to roll process, Nanoscale 4 (2012) 6032–6040.

[106] Y. Galagan, R. Andriesse, Organic Photovoltaics: Technologies and Manufacturing Technologies, Third generation photovoltaics, intech open, New York, 2012, 8.

[107] S.H. Eom, S. Sundaram, S.C. Yoon, J. Lee, S.H. Lee, Nanoscale ZnO buffer layer for inkjet printed polymer solar cells, J. Nanosci. Nanotechnol. 8 (2008) 5113–5117.

[108] F. Wang, Z. Tan, Y. Li, Solution processable metal oxides/chelates as electrode buffer layers for efficient and stable polymer solar cells, Energy Environ. Sci. 8 (2015) 1059–1091.

[109] H. Zheng, Y. Zheng, N. Liu, N. Ai, Q. Wang, S. Wu, J. Zhou, D. Hu, S. Yu, S. Han, W. Xu, C. LuO, Y. Meng, Z. Jiang, Y. Chen, D. Li, J. Peng, C.O. Yong, All solution processed polymer light emitting diode displays, Nat. Commun. 4 (1971) (2013) 1–6.

[110] M. Hosel, R.R. Sondergaard, D. Angmo, F.C. krebs, Comparison of fast roll to roll flexographic, inkjet, flatbed and rotary screen printing of metal back electrodes for polymer solar cells, Sol. Energy Mater. Sol. Cells l15 (2013) 995–1001.

[111] J. Kim, N. Durai, T.M. Lee, I. Kim, K.H. Choi, Screen printed top electrode for efficient inverted organic solar cells, Mater. Res. Bull. 70 (2015) 412–415.

[112] F.C. krebs, H. Spanggard, T. Kjaer, M. Biancardo, J. Alstrup, Large area plastic solar cell modules, Mater Sci Eng B 138 (2007) 106–111.

[113] H. Yakup, S. Sait Eren, O. Teo man, A. Erdem, C. Hasip, S. Huseyin, Manufacturing of Inorganic-Organic Hybrid Solar Cells by Screen Printing Method, 6th Nanoscience and Nanotechnology Conference, (NanoTRVI) Izmir, Turkey, 2010.

[114] B. Zhang, H. Chae, S.M. Cho, Screen printed polymer fullerene bulk heterojunction polymer solar cells, Jpn. J. Appl. Phys. 48 (2009), 020208.

[115] T.T. Olsen, R.R. Sondergaard, K. Norman, M. Jorgensen, F.C. Krebs, All printed transparent electrodes through an electrical switching mechanism: a convincing alternative to indium tin oxide, silver and vacuum, Energy Environ. Sci. 5 (2015) 9467–9471.

[116] T.R. Andersen, T.T.L. Olsen, B. Andreasen, A.P.L. Bottiger, J.E.C.M. Helgesen, E. Bundgaard, K. Norrman, J.W. Andreasen, M. Jorgensen, F.C. krebs, Aqueous processing of low bandgap polymer solar cells using Roll-to-Roll methods, ACS Nano. 5 (2011) 4188–4196.

[117] R. Sondergaard, M. Helgesen, M. Jorgensen, F.C. Krebs, Fabrication of polymer solar cells using aqueous processing for all layers including the metal back electrode, Adv. Energy Mater. 1 (2011) 68–71.

[118] F.C. Krebs, Polymer solar cell modules prepared using roll-roll-methods: knife -over-edge coating,slot-die coating and screen printing, Sol. Energy Mater. Sol. Cells 93 (2009) 465–475.

[119] L.S. Pali, R. Jindal, A. Garg, Screen printed PEDOT:PSS films as transparent electrode and its appplications in organic solar cells on opaque substrates, J. Mater Sci: Mater Electron. 29 (2018) 11030–11038.

[120] T. Aernouts, T. Aleksandrov, C.G.J. Genoe, J. Poortmans, Polymer based organic solarcells using inkjet printed active layers, App. Phys. Lett. 92 (1–3) (2008) 033306.

[121] A.D.G.D. Mauro, R. Diana, A. Grimaldi, F. Loffredo, P. Morvillo, F. Villani, C. Minarini, Polymer Solar Cells With Inkjet Printed a Doped PEDOT:PSS Anode, Presented at the 6th Conference on the Times of Polymers & Composites Held at Ischia Italy, 2012.

[122] Y.C. Huang, F.H. Hsu, H.C. Cha, C.M. Chuang, C.S. Tsao, C.Y. Chen, High performance ITO-free spray-processed polymer solar cells with incorporating ink-printed grid, Org. Electron. 14 (2013) 2809–2817.

[123] M. Neophytou, F. Hermerschmidt, A. Savva, E. Georgiou, S.A. Choulis, Highly efficient indium tin oxide free organic photovoltaics using inkjet printed silcer nanoparticle current collecting grids, Appl. Phys. Lett. 101 (2012) 193302.

[124] E. Georgiou, S.A. Choulis, Felix Hermerschmidt, S.M. Pozov, I.B. Ceballos, C. Christodoulou, G. Schider, S. Kressi, R. Ward, E.J.W.L. Kratochvil, C. Boeffel, Printed copper nanoparticle metal grids for cost effective ITO-free solution processed solar cells, Sol. RRL 2 (2018) 1700192.

[125] S.H. Eom, H. Park, S.H. Mujawar, S.C. Yoon, S.S. Kim, S.I. Na, S.J. Kang, D. Khim, D.Y. Kim, S.H. Lee, High efficiency polymer solar cells via sequential inkjet printing of PEDOT:PSS and P3HT:PCBM with additives, Org. Electron. 11 (2010) 1516–1522.

[126] Y. Galagan, E.W.C. Coenen, S. Sabik, H.H. Gorter, M. Barink, S.C. Veenstra, J.M. Kroon, R. Andriessen, P.W.M. Blom, Evaluation of inkjet printed current collecting grids and busbars for ITO free organic solar cells, Energy Mater. Sol. Cells 104 (2012) 32–38.

[127] J. Kim, S.I. Na, H.K. Kim, Inkjet printing of transparent InZnSnO conducting electrodes from nano-particle ink for printable organic photovoltaics, Sol. Energy Mater. Sol. Cells 98 (2012) 424–432.

[128] H.K. Kim, I.K. You, J.B. Koo, S.K. Kim, Organic solar cells fabricated on inkjet printed tin oxide electrodes, Surf. Coat. Tech. 211 (2012) 33–36.

[129] S. Sankaran, K. Glaser, S. Gartner, T. Rodlmeier, K. Sudau, G.H. Sosa, A. Colsmann, Fabrication of polymer solar cells from organic nanoparticle dispersions by doctor blading or inkjet printing, Org. Electron. 28 (2016) 118–122.

[130] T.M. Eggenhuisen, Y. Galagan, A.F.K.V. Biezemans, T.M.W.L. Slaats, W.P. Voorthuijzen, S. Kommeren, S. Shanmugam, J.P. Teunissen, A. Hadipour, W.J.H. Verhees, S.C. Veenstra, M.J.J. Coenen, J. Gilot, R. Andriessen, W.A. Groen, High efficiency fully inkjet printed organic solar cells with freedom of design, J. Mater.Chem. A 3 (2015) 7255–7262.

[131] P. Maisch, K.C. Tam, L. Lucera, H.J. Egelhaaf, H. Scheiber, E. Maier, C.J. Brabec, Inkjet printed silver nanowire percolation networks as electrodes for highly efficient semitransparent organic solar cells, Org. Electron. 38 (2016) 139–143.